Parametric Amplifiers for Optical Coherent Communication

A Project Report

submitted by

KARTHIK VIJAY ANNUR MYILSWAMY

in partial fulfilment of the requirements
for the award of the degree of

BACHELOR AND MASTER OF TECHNOLOGY

DEPARTMENT OF ELECTRICAL ENGINEERING
INDIAN INSTITUTE OF TECHNOLOGY MADRAS.

May 2019

THESIS CERTIFICATE

This is to certify that the thesis titled **Parametric amplifers for optical coherent communication**, submitted by **Karthik Vijay Annur Myilswamy**, to the Indian Institute of Technology, Madras, for the award of the degree of **Bachelor and Master of Technology**, is a bona fide record of the research work done by him under our supervision. The contents of this thesis, in full or in parts, have not been submitted to any other Institute or University for the award of any degree or diploma.

Prof. Deepa Venkitesh
Research Guide
Associate Professor
Dept. of Electrical Engineering
IIT-Madras, 600 036

Place: Chennai

Date: May 05, 2019

ACKNOWLEDGEMENTS

I would like to sincerely thank Prof. Deepa Venkitesh for being a dedicated and motivating guide. The freedom I had to explore the research topics that intrigued me is owed to her. I would like to thank her for especially for the dedicated weekly meetings which helped me shape this project significantly. I am extremely fortunate to have been a part of the Optical communication and Network (OCEAN) lab. The experimental resources provided in this lab aided significantly in the completion of this work. Working in this lab has given me a rich insight into research and academia, which motivated me to pursue academic research in the field further.

I would also like to extend my thanks to my mentor Aneesh Sobhanan who helped me get over many obstacles in the experimental work and shared his expertise. I also convey my special thanks to Anirudh Vijay, who was always with me in this beautiful journey at IITM. I am happy to have worked with him on the SOA simulations. I thank my other lab mates from Ocean lab for making the lab a fun and lively place to work in.

I would also like to extend my gratitude to my classmates and friends for being a strong pillar of support while I worked on my project.

ABSTRACT

KEYWORDS: Fiber optic parametric amplification; Phase insensitive (PIA) and phase sensitive (PSA) amplification; SBS suppression; SOA; MSSI

The necessity of operating long haul optical commuincation links under higher OSNR conditions has renewed the research interests in fiber optic parametric amplifiers (FOPA), especially phase sensitive amplification. Phase sensitive amplification (PSA) promises a noise figure of $-3\ dB$ compared to typical $3\ dB$ quantum limit of Erbium doped fiber amplifiers (EDFA). The challenges in realising PSA in fibers lies in the complexity of the setup arising from stimulated Brillouin scattering and phase locking of signal, pump and idler waves. This report focuses on the theoretical analysis of PSA and PIA, and the experimental realisation of the same using phase modulation for SBS suppression. This report also evaluates SOA as a potential competitor for amplification and phase conjugation for coherent optical communication.

TABLE OF CONTENTS

LIST OF TABLES

LIST OF FIGURES

ABBREVIATIONS

ASE	Amplified Spontaneous Emission
AWGN	Additive White Gaussian Noise
BER	Bit Error Rate
BPF	Band Pass Filter
CDC	Chromatic Dispersion Compensation
EDFA	Erbium Doped Fiber Amplifier
EVM	Error Vector Magnitude
HNLF	Highly Non-Linear Fiber
FOPA	Fiber Optic Parametric Amplifier
FWM	Four Wave Mixing
GVD	Group Velocity Dispersion
MSSI	Mid-Span Spectral Inversion
NF	Noise Figure
NLSE	Nonlinear Schrodinger Equation
OPC	Optical Phase Conjugation
OSNR	Optical Signal to Noise Ratio
PA	Parametric Amplification
PIA	Phase Insensitive Amplification
PSA	Phase Sensitive Amplification
QAM	Quadrature Amplitude Modulation
QPSK	Quadrature Phase Shift Keying
SBS	Stimulated Brillouin Scattering
SMF	Single Mode Fiber
SNR	Signal to Noise Ratio
SPM	Self Phase Modulation
THG	Third Harmonic Generation
WDM	Wavelength Division Multiplexing
XPM	Cross Phase Modulation

NOTATION

$\vec{E(t)}$	Electric field
$\vec{P(t)}$	Induced polarization in dielectric medium
h	Planck's constant
c	Speed of light in vacuum
ϵ_0	Free space permittivity
$\chi^{(i)}$	$i^{th}-$order susceptibility tensor
ϵ_r	Relative permittivity
n	Refractive index
$c.c.$	Complex conjugate
n_0	Linear refractive index
n_2	Kerr coefficient
γ	Nonlinear parameter
A_{eff}	Effective modal area
z	Space coordinate
t	Time coordinate
$A(z,T)$	Slowly varying envelope
β_1	Group velocity
β_2	Group velocity dispersion
α	Attenuation coefficient of fiber
D	Dispersion parameter
G_{PIA}	Signal gain in phase insensitive amplification
G_{PSA}	Signal gain in phase sensitive amplification
η	Idler conversion efficiency
V_π	Half-wave voltage of phase modulator
P_p	Pump power
P_s	Signal Power
λ_p	Pump wavelength
λ_s	Signal wavelength
f_p	Pump frequency
f_s	Signal frequency
Δf_p	Pump linewidth
Δf_s	Signal linewidth

CHAPTER 1

Introduction

Increase in the demand for higher data rates or throughput (Jung (2011), Index (2017)) requires to drive the performance of communication links closer to the Shannon capacity (Cover and Thomas (2012)). This has necessitated the practical realization of the following in the long haul optical communication links: usage of advanced modulation formats and the usage of multiple channels in parallel like wavelength, time or space division multiplexing. The bit error rate (BER) versus optical signal-to-noise ratio (OSNR) for different modulation formats in AWGN channel are plotted in Figure 1.1 for a datarate of $20\ GBd$ (Proakis (2001)). It can be observed that the usage of higher modulation formats requires higher OSNR. This associated requirement of operating under higher OSNR conditions makes the role of low noise amplifiers with wide bandwidth critical in long haul optical systems (Karlsson (2016)).

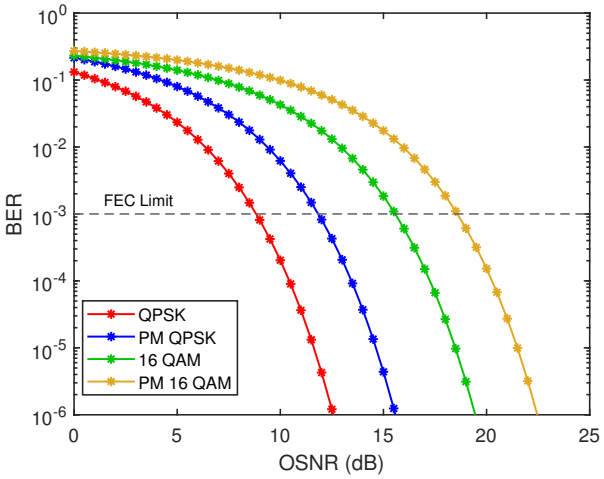

Figure 1.1: BER vs OSNR for different advanced modulation formats for $20\ GBd$ datarate; PM refers to polarization multiplexing

Erbium doped fiber amplifiers (EDFA) are by far the most extensively employed optical amplifiers in the long haul transmission links as they can efficiently provide an amplification of $>\ 20\ dB$ in the telecommunication wavelength range (Mears *et al.* (1987)). One of the main advantages of EDFA is its wide optical gain bandwidth. Both of the Conventional, or C-band ($1525\ nm - 1565\ nm$) and the Long, or L-band

($1570\ nm - 1610\ nm$) can be effectually amplified using EDFAs (Emmanuel and Zervas (1994)). High gain and polarization independence are the other major benefits that led to the wide-spread usage of EDFAs in optical links. However, the noise figure of EDFA is slightly larger than that of the $3\ dB$ quantum limit in the high gain regime (Pedersen *et al.* (1991), Abedin *et al.* (2011)). Commercial EDFAs typically are available with $6\ dB$ noise figure for a small signal gain of $35\ dB$ and a saturated output power of $23\ dBm$ (PriTel Inc (2005)).

Fiber optic parametric amplifiers (FOPAs) that rely on Kerr nonlinearity in fibers have attracted the research interest as they provide flat gain, broad bandwidth, ultrafast response, uni-directionality and especially operation outside the EDFA bands (Agrawal (2000)). In addition to this, FOPAs are good candidates for several other optical signal processing techniques that include wavelength conversion, phase conjugation and phase regeneration (Hansryd *et al.* (2002), Kurosu *et al.* (2015), Hu *et al.* (2010), Lali-Dastjerdi *et al.* (2013)). Parametric amplifiers have the distinct ability to be operated in two different modes: phase insensitive amplification (PIA) and phase sensitive amplification (PSA). PIA have a $3\ dB$ quantum noise figure limit in the high gain regime, similar to that of EDFAs. However, it is possible to achieve $0\ dB$ noise figure in PSA, owing to the coherent superposition of signal and idler waves in nonlinear medium. This property of PSA in FOPAs, thus can be exploited for achieving low noise amplification in communication links.

The main drawback of PSA is the complexity of the setup arising from the requirement of achieving phase matching between pump, signal and idler waves at the input of FOPA stage. Also in case of WDM scenario, parametric amplification can lead to severe nonlinear crosstalk between multiple WDM channels, that is highly detrimental. In order to reduce this nonlinear crosstalk, techniques such as maintaining high pump to signal ratio have been proposed (Jamshidifar *et al.* (2009)). One of the other primary limitations of FOPA is stimulated Brillouin scattering, that limits the pump power that can be launched into the optical fiber. Several active techniques such as phase modulation and passive techniques such as temperature or strain gradient along the length of fiber have been proposed in the past to increase the SBS threshold (Grüner-Nielsen *et al.* (2010), Coles *et al.* (2010)), which again increases the complexity of the system rendering it difficult for implementation in real-time systems. This renews the interest in non-parametric nonlinear media such as semiconductor optical amplifiers (SOAs)

that can be used for effective realization of PIA and PSA. SOA offers several other advantages such as compactness, power efficiency etc compared to HNLF, which are elucidated in the later part of the report. Hence, nonlinearity based optical amplifier, being one of the fundamental building blocks of the transmission link, is the primary focus of this report. The organisation of this report is as follows.

Chapter 2 presents the theory of Kerr nonlinearity in fibers that has been constructively exploited for parametric amplification in FOPAs. In Section 2.2, the theoretical analysis of gain and noise properties of PIA and PSA in HNLF is presented. The dependence of PIA and PSA on dispersion, nonlinearity and pump power in degenerate pump configuration is explained in Section 2.3. Section 2.4 introduces the reader to SBS in optical fibers and the mitigation strategies that have been proposed in the past to suppress the same.

Chapter 3 presents the experimental results of SBS suppression using phase modulation of pump and parametric amplification in degenerate pump configuration in HNLF. It also sets the motivation to employ dual pump configuration using counter phase modulation for SBS suppression and presents the theoretical analysis and experimental results of the same in Section 3.3.

Chapter 4 presents the advantages of SOA compared to that of HNLF for nonlinear applications. In Section 4.1, the analytical model of SOA is explained and the simulation results of PIA and PSA have been presented. The simulation results of QPSK modulated signals in SOA and their performance have been discussed in Section 4.2 to set the motivation for employing SOAs in long haul optical links. Section 4.3 identifies mid-span spectral inversion (MSSI) using phase conjugation as one of the potential ways of compensating chromatic dispersion and nonlinearity impairments in long haul transmission links and the performance of MSSI using SOA is analysed in Section 4.3.1.

Chapter 5 concludes the report and presents the scope for future work.

CHAPTER 2

Fiber Optic Parametric Amplifiers

Parametric amplification is a phenomenon in which a signal wave is amplified utilizing the parametric nonlinear properties of the optical medium in the presence of a pump wave. It does not involve any excitation of the atoms/ charge carriers to higher energy levels that results in stimulated amplification of the signal. It rather exploits the behaviour of light in nonlinear media in which the energy redistribution happens among different frequencies due to the modulation of the refractive index of the medium. The nonlinear response of the optical medium is almost instantaneous which is used for different applications including wavelength conversion, phase conjugation, phase quantization, super-continuum generation, optical switching, parametric amplification and oscillation.

Parametric nonlinearities arise from the interaction of the optical signal with the bound charges present in the dielectric material. The oscillating electric field of an optical signal induces dipole moment in a dielectric material and thus induces dielectric polarization. The induced polarization ($\vec{P(t)}$) in a dielectric material due to the electric field ($\vec{E(t)}$) is given by the following power series relation:

$$\vec{P(t)} = \epsilon_0(\chi^{(1)}\vec{E(t)} + \chi^{(2)} : \vec{E(t)}\vec{E(t)} + \chi^{(3)} : \vec{E(t)}\vec{E(t)}\vec{E(t)} + ...) \tag{2.1}$$

where ϵ_0 is the permittivity of the free space and $\chi^{(i)}$ are the i^{th} order susceptibilities of the dielectric medium. $\chi^{(i)}$ are tensors of rank $(i+1)$ and determine whether the material response is linear or nonlinear to the electric field of the applied optical signal. The complex value of $\chi^{(i)}$ determines the phase, gain or loss that the optical signal undergoes in the dielectric material medium. $\chi^{(1)}$ describes the linear response of the dielectric medium. The relative permittivity of the linear dielectric medium depends on the first order susceptibility and is expressed by the following relation.

$$\epsilon_r = n^2 = 1 + \chi^{(1)} \tag{2.2}$$

2.1 Nonlinear effects in Highly Non-Linear Fiber

The even order susceptibilities are absent in silica fibers owing to its centrosymmetric crystal structure (Agrawal (2000)). Hence, third order susceptibility $(\chi^{(3)})$ primarily contributes to the nonlinear effects in the fiber. The different effects due to $\chi^{(3)}$ nonlinearity can be clearly explained by considering an electric filed comprising of three different frequency components:

$$\vec{E} = \frac{1}{2}\left(\sum_{i=1}^{3} \vec{E}_i \; e^{j(\omega_i t - k_i z)} + c.c.\right) \tag{2.3}$$

where $c.c.$ refers to the complex conjugate. The third order terms ($\vec{P}^{(3)}$) in the induced polarization due to $\chi^{(3)}$ susceptibility in the fiber for the above mentioned electric filed (see equation 2.3) can be expressed as:

$$\begin{aligned}
\vec{P}^{(3)} = {} & \frac{3}{4}\epsilon_0\chi^{(3)}[\ |\vec{E}_1|^2\vec{E}_1\ e^{j(\omega_1 t - k_1 z)} + \diamond\ ] && \textit{(SPM)} \\
& + \frac{6}{4}\epsilon_0\chi^{(3)}[\ (|\vec{E}_2|^2 + |\vec{E}_3|^2)\vec{E}_1\ e^{j(\omega_1 t - k_1 z)} + \diamond\ ] && \textit{(XPM)} \\
& + \frac{1}{4}\epsilon_0\chi^{(3)}[\ (\vec{E_1}^{\,3}\ e^{j(3\omega_1 t - 3k_1 z)} + c.c.) + \diamond\ ] && \textit{(THG)} \\
& + \frac{3}{4}\epsilon_0\chi^{(3)}[\ \frac{1}{2}(\vec{E_1}^{\,2}\vec{E}_2\ e^{j(2\omega_1+\omega_2)t - (2k_1+k_2)z)} + c.c.) + \diamond\ ] && \textit{(FWM)} \\
& + \frac{3}{4}\epsilon_0\chi^{(3)}[\ \frac{1}{2}(\vec{E_1}^{\,2}\vec{E}_2^{*}\ e^{j(2\omega_1-\omega_2)t - (2k_1-k_2)z)} + c.c.) + \diamond\ ] && \textit{(FWM)} \\
& + \frac{6}{4}\epsilon_0\chi^{(3)}[\ \frac{1}{2}(\vec{E}_1\vec{E}_2\vec{E}_3\ e^{j(\omega_1+\omega_2+\omega_3)t - (k_1+k_2+k_3)z)} + c.c.) + \diamond\ ] && \textit{(FWM)} \\
& + \frac{6}{4}\epsilon_0\chi^{(3)}[\ \frac{1}{2}(\vec{E}_1\vec{E}_2\vec{E}_3^{*}\ e^{j(\omega_1+\omega_2-\omega_3)t - (k_1+k_2-k_3)z)} + c.c.) + \diamond\ ] && \textit{(FWM)}
\end{aligned} \tag{2.4}$$

where $\diamond$ represents all possible similar permutations. The first term on the right-hand side of the equation 2.4 refers to the self phase modulation (SPM) phenomenon where the signal at ω_i modulates the refractive index experienced by the signal at ω_i itself. The second term on the right-hand side of the equation 2.4 refers to the cross phase modulation (XPM) phenomenon where the signal at ω_i influences the refractive index change experienced by the other signal frequencies $\omega_{j(j\neq i)}$ in the medium. The refractive index modulation due to XPM is twice as strong as that of SPM. SPM and XPM contribute to the intensity dependent refractive index change of the medium and determines the total nonlinear phase shift that the signal undergoes in the dielectric media in addition to the dispersive phase shift. The third term on the right hand side

of the equation 2.4 corresponds to the third harmonic generation (THG) at frequencies $3\omega_i$ from respective signals at frequencies ω_i. The rest of the terms in equation 2.4 correspond to four wave mixing (FWM) where three incident waves interact with each other and results in a formation of the fourth idler wave. FWM is responsible for many nonlinear phenomena including parametric amplification, phase conjugation and wavelength conversion. Among the many nonlinear interactions, only those satisfy both energy conservation and momentum conservation (phase matching) are effective. The strength of the nonlinear interactions primarily depends on the following factors:

- intensity of the optical field
- Kerr coefficient ($n_2 = \frac{3\chi^{(3)}}{4n_0^2}$) of the dielectric media, where n_0 is the linear refractive index
- phase matching incorporating both dispersive and nonlinear phase shift into account

Another useful parameter that is generally defined in nonlinear optics context is nonlinear parameter γ which helps to quantify the nonlinear interactions more effectively and is expressed as

$$\gamma = \frac{2\pi}{\lambda}\frac{n_2}{A_{eff}} \tag{2.5}$$

where λ represents the wavelength and A_{eff} refers to the effective modal area of the fiber. It can be noted that the nonlinear parameter γ increases with the Kerr coefficient (n_2) of the dielectric medium. Also, the nonlinear parameter increases with the intensity of the optical field which corresponds to that of decrease in the effective modal area of the fiber. For a typical single mode fiber (SMF) G.652, which is by far the most widely used fiber in the optical communication links globally, the effective modal area is $\approx 80\ \mu m^2$ and the nonlinear parameter (γ) is $1.7\ W^{-1}km^{-1}$. It requires optical power in the order of few watts to instigate effective parametri nonlinear interactions in SMF G.652, which is highly preferred in WDM communication links because of negligible inter channel interference. However, it is highly imperative to have a fiber design with higher nonlinearity to efficiently realize various nonlinear applications including phase conjugation and parametric amplification. The design of Highly Non-Linear Fiber (HNLF) includes a high delta core surrounded by a deeply depressed ring and doped with Fluorine that results in an increased nonlinear coefficient (γ) of around $11.1\ W^{-1}km^{-1}$. Hence, it requires only a few hundreds of milliwatts of optical power

to instigate efficient nonlinear interactions in HNLF and is heavily employed in various nonlinear optical signal processing systems (Shao and Kumar (2012), Hu *et al.* (2015), Liu *et al.* (2010)).

2.2 Parametric amplification in HNLF

As explained in the previous section (see Section 2.1), FWM is conversion of energy between different frequencies in an energy preserving manner, that can be used for various applications in optical communication links. The following discussion is primarily focused on parametric amplification where the energy is transferred from the stronger pump waves to the weaker signal and idler waves. Depending on the pump, signal and idler frequencies, the FWM process can either be degenerate or non-degenerate. When two pump photons at the same frequency ω_p give rise to a signal photon at frequency ω_s and an idler photon at frequency ω_i as shown in Fig. 2.1a, the FWM process is said to have degenerate pump configuration. The energy conversion for degenerate pump configuration is expressed by $2\omega_p = \omega_s + \omega_i$. In case of non-degenerate or dual pump configuration as shown in Fig. 2.1b, two pump photons at different frequencies ω_{p1} and ω_{p2} give rise to a signal photon at frequency ω_s and an idler photon at frequency ω_i. The energy conversion in dual pump configuration is described by $\omega_{p1} + \omega_{p2} = \omega_s + \omega_i$.

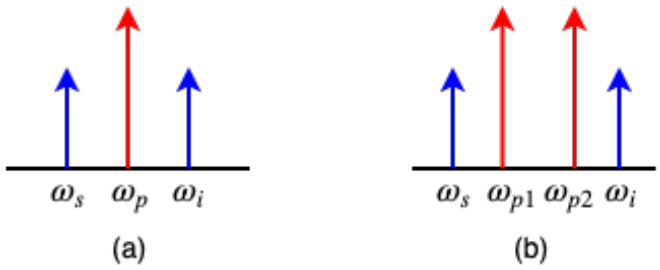

Figure 2.1: Schematic spectra of FWM with (a) degenerate pump, (b) dual pump

2.2.1 Theory of four wave mixing

Four wave mixing can be analysed using Nonlinear Schrodinger equation (NLSE) which is used to model the propagation of light in optical fibers. The propagation of the slowly varying envelope $A(z,T)$ of the optical signal oscillating around ω_0 in fiber is expressed

using NLSE as

$$\frac{\partial A}{\partial z} + j\frac{\beta_2}{2}\frac{\partial A}{\partial T} = j\gamma|A|^2A - \alpha\frac{A}{2} \tag{2.6}$$

where z, T correspond to the space and time coordinates, $\beta_m = (\frac{d^m\beta}{d\omega^m})_{\omega=\omega_0}$ correspond to the terms in Taylor series expansion of the wavenumber $\beta(\omega)$ around ω_0 and α denotes the attenuation coefficient of the fiber. The optical signal propagates with a group velocity of β_1 in the fiber. A frame of reference ($T = t - \beta_1 z$) that is moving along with the pulse at group velocity is considered in equation 2.6. The parameter β_2 describes the frequency dependence of group velocity and this phenomenon is called group velocity dispersion (GVD). Dispersion parameter (D) which is most widely used in fiber optics context is related to β_2 as $D = -\frac{2\pi c}{\lambda^2}\beta_2$. Dispersion in optical fibers depends on both material and waveguide characteristics.

The propagation of four waves at oscillating at frequencies $(\omega_{p1}, \omega_{p2}, \omega_s, \omega_i)$ through the fiber can be explained using the following set of coupled equations obtained from NLSE equation 2.6 as

$$\begin{aligned}
\frac{dA_{p1}}{dz} &= j\gamma(|A_{p1}|^2 + 2|A_{p2}|^2 + 2|A_s|^2 + 2|A_i|^2)A_{p1}) + 2A_sA_iA_{p2}^*e^{j\Delta\beta z} \\
\frac{dA_{p2}}{dz} &= j\gamma(2|A_{p1}|^2 + |A_{p2}|^2 + 2|A_s|^2 + 2|A_i|^2)A_{p2}) + 2A_sA_iA_{p1}^*e^{j\Delta\beta z} \\
\frac{dA_s}{dz} &= j\gamma(2|A_{p1}|^2 + 2|A_{p2}|^2 + |A_s|^2 + 2|A_i|^2)A_s) + 2A_{p1}A_{p2}A_i^*e^{-j\Delta\beta z} \\
\frac{dA_i}{dz} &= j\gamma(2|A_{p1}|^2 + 2|A_{p2}|^2 + 2|A_s|^2 + |A_i|^2)A_i) + 2A_{p1}A_{p2}A_s^*e^{-j\Delta\beta z}
\end{aligned} \tag{2.7}$$

where wave vector mismatch $\Delta\beta$ is given by $\Delta\beta = \beta_s + \beta_i - \beta_{p1} - \beta_{p2}$.

Generally, the pump powers (P_{p1}, P_{p2}) are very high compared to that of signal power (P_s) and idler power (P_i). Hence, it can be assumed that the pump waves undergo negligible depletion for obtaining analytical expressions and this approximation is referred to as undepleted pump approximation ($P_{p1}, P_{p2} >> P_s, P_i$). Considering $A_{s,i} = B_{s,i}e^{j\kappa z}$, the amplitude of the signal and the idler at the output can be found by solving the following pair of coupled equations (see equation 2.8), under undepleted pump approximation assumptions (Karlsson (2016)).

$$\frac{d}{dz}\begin{bmatrix} B_s(z) \\ B_i^*(z) \end{bmatrix} = j\begin{bmatrix} \kappa & 2\gamma\sqrt{P_{p1}P_{p2}} \\ -2\gamma\sqrt{P_{p1}P_{p2}} & -\kappa \end{bmatrix}\begin{bmatrix} B_s(0) \\ B_i^*(0) \end{bmatrix} = M\begin{bmatrix} B_s(0) \\ B_i^*(0) \end{bmatrix} \tag{2.8}$$

where M is the coefficient matrix. The solution of equation 2.8 can be obtained as

$$\begin{bmatrix} B_s(z) \\ B_i^*(z) \end{bmatrix} = e^{jzM} \begin{bmatrix} B_s(0) \\ B_i^*(0) \end{bmatrix} \tag{2.9}$$

$$\begin{bmatrix} B_s(z) \\ B_i^*(z) \end{bmatrix} = \begin{bmatrix} cosh(gz) + j\frac{\kappa}{g}sinh(gz) & j\frac{2\gamma\sqrt{P_{p1}P_{p2}}}{g}sinh(gz) \\ -j\frac{2\gamma\sqrt{P_{p1}P_{p2}}}{g}sinh(gz) & cosh(gz) - j\frac{\kappa}{g}sinh(gz) \end{bmatrix} \begin{bmatrix} B_s(0) \\ B_i^*(0) \end{bmatrix} \tag{2.10}$$

where $2\kappa = \Delta\beta + \gamma(P_{p1} + P_{p2})$ is the net phase mismatch. The net phase mismatch has two components: dispersive phase mismatch ($\Delta\beta$) and nonlinear phase mismatch ($\gamma(P_{p1} + P_{p2})$). The nonlinear phase mismatch is the consequence of SPM and XPM in the optical fiber. Here, $g = \sqrt{(4\gamma P_{p1}P_{p2}) - \kappa^2}$ is the parametric gain coefficient. The parametric gain coefficient (g) is maximised when the net phase mismatch (2κ) is zero. The net phase mismatch can be reduced to zero only when the nonlinear phase mismatch cancels the dispersive phase mismatch.

2.2.2 Phase insensitive and phase sensitive gain

The properties of the transfer matrix $K(z)$ should be established to understand the gain and noise properties of the parametric amplifier. It can be obtained from equation 2.10 that, the transfer matrix $K(z)$ assumes the following form

$$K = \begin{bmatrix} \mu & \nu \\ \nu^* & \mu^* \end{bmatrix} \tag{2.11}$$

where μ, ν are complex coefficients such that $|\mu|^2 - |\nu|^2 = 1$.

In the absence of idler wave at the input, equation 2.10 can be expressed using equation 2.11 as

$$\begin{bmatrix} B_s(z) \\ B_i^*(z) \end{bmatrix} = \begin{bmatrix} \mu & \nu \\ \nu^* & \mu^* \end{bmatrix} \begin{bmatrix} B_s(0) \\ 0 \end{bmatrix} \tag{2.12}$$

From equation 2.12, it can be noted that the signal experiences a gain of $G_{PIA} = \left|\frac{B_s(z)}{B_s(0)}\right|^2 = |\mu|^2$ and the idler conversion efficiency is $\eta = \left|\frac{B_i(z)}{B_s(0)}\right|^2 = |\nu|^2 = G_{PIA} - 1$.

The absolute phases of the complex coefficients μ, ν, signal and idler waves do not influence the gain experienced by the signal in the absence of idler at the input. Hence, the signal undergoes phase insensitive amplification in the absence of idler at the input. Also, the generated idler is phase conjugated version of the signal. If both signal and idler waves are present at the input, the interaction between the different waves becomes phase sensitive. From equations 2.10 and 2.11, the output waves can be expressed as

$$\begin{aligned} B_s(z) &= \mu B_s(0) + \nu B_i^*(0) \\ B_i^*(z) &= \nu^* B_s(0) + \mu^* B_i(0) \end{aligned} \tag{2.13}$$

The gain experienced by the signal in phase sensitive case is given by the following relation

$$G_{PSA} = \left| \frac{B_s(z)}{B_s(0)} \right|^2 = \frac{|\mu B_s(0) + \nu B_i^*(0)|^2}{|B_s(0)|^2} \tag{2.14}$$

If the signal and idler powers are equal at the input, the phase sensitive signal gain is given by

$$G_{PSA} = |\mu|^2 + |\nu|^2 + 2|\mu||\nu| cos(\phi) \tag{2.15}$$

where $\phi = \phi_s + \phi_i - \phi_{p1} - \phi_{p2} + \angle\mu - \angle\nu$. It can be seen that the parametric gain experienced by the signal depends on the input phase of the pump, signal and idler waves. It is also important to have phase locking between pump, signal and idler waves at the input so that ϕ_s, ϕ_i, ϕ_{p1} and ϕ_{p2} are not independently time varying. The phase locked waves can be generated from frequency comb source or by using another parametric amplifier (copier) stage to generate phase locked idler from signal and pump waves.

The signal experiences a maximum gain of $G_{max,PSA} = (|\mu| + |\nu|)^2$ if $\phi = 2m\pi$ and a minimum gain of $G_{min,PSA} = (|\mu| - |\nu|)^2$ if $\phi = (2m+1)\pi$, where m is an integer. From the properties of the transfer matrix mention in equation 2.11, it can be inferred that $G_{max,PSA} = \frac{1}{G_{min,PSA}}$. This means that the signal components which satisfy the phase relation $-\frac{\pi}{2} + 2m\pi < \phi < \frac{\pi}{2} + 2m\pi$ undergo amplification whereas the signal components which satisfy the phase relation $-\pi + 2m\pi < \phi < -\frac{\pi}{2} + 2m\pi$ or $\frac{\pi}{2} + 2m\pi < \phi < \pi + 2m\pi$ undergo attenuation. This property of phase sensitive amplification has been efficaciously exploited in various applications including phase regeneration (Kurosu *et al.* (2015)) and phase squeezing (Puttnam *et al.* (2011)). Also, the maximum phase sensitive gain is approximately $G_{max,PSA} \approx 4|\mu|^2 \equiv 4G_{PIA}$, showing the $6\ dB$ difference between the PIA and PSA gain. This is due to the coherent

superposition of the signal and idler waves resulting in a 4-fold increase in gain.

2.2.3 Noise figure in PIA and PSA

The noise figure is defined as the ratio $NF = \frac{SNR_{in}}{SNR_{out}}$. Lets assume that the input signal has an amplitude of $B_{s,in}$ and a noise amplitude of n_s with a power spectral density of $S_{s,in} =< |n_s|^2 >$. In the photo-detection process, the noise has two different components: signal-noise beating and noise-noise beating in the shot noise dominating regime. Noise-noise beating can be neglected in comparison with signal-noise beating. Under that assumption, the SNR of the signal at the input is given by (Olsson (1989))

$$SNR_{in} = \frac{(RP_{s,in})^2}{4R^2 P_{s,in} S_{s,in} \Delta f} = \frac{P_{s,in}}{4S_{s,in}\Delta f} = \frac{|B_{s,in}|^2}{4S_{s,in}\Delta f} \tag{2.16}$$

where R corresponds to the responsivity of the photodiode, $P_{s,in}$ denotes the input signal power and Δf is the electric bandwidth.

In case of parametric amplification, the output signal field can be expressed using equation 2.11 as

$$\begin{aligned} B_{s,out} &= \mu(B_{s,in} + n_s) + \nu(B^*_{i,in} + n_i) \\ B_{s,out} &= (\mu B_{s,in} + \nu B^*_{i,in}) + (\mu n_s + \nu n_i) \end{aligned} \tag{2.17}$$

where $B_{i,in}$ and n_i correspond to signal and noise amplitudes of the idler wave at the input. If the power spectral density of noise at both signal and idler frequencies are assumed to be equal at the input ($S_{i,in} = S_{s,in} = S_{in}$), the power spectral density of the noise at the output ($S_{s,out}$) is given by the following relation

$$S_{s,out} =< |\mu n_s + \nu n_i|^2 >= (|\mu|^2 + |\nu|^2) S_{in} \tag{2.18}$$

as the noise at signal and idler frequencies are uncorrelated which dictates the SNR of the signal at the output to be

$$SNR_{s,out} = \frac{(RP_{s,out})^2}{4R^2 P_{s,out} S_{s,out} \Delta f} = \frac{P_{s,out}}{4S_{s,out}\Delta f} = \frac{|(\mu B_{s,in} + \nu B^*_{i,in})|^2}{4(|\mu|^2 + |\nu|^2) S_{in} \Delta f} \tag{2.19}$$

From the equations 2.16 and 2.19, the noise figure associated with the parametric am-

plification process is finally obtained as the following relation

$$NF_s = \frac{SNR_{s,in}}{SNR_{s,out}} = \frac{(|\mu|^2 + |\nu|^2)|B_{s,in}|^2}{|(\mu B_{s,in} + \nu B^*_{i,in})|^2} \tag{2.20}$$

In case of phase insensitive amplification, where the idler wave is absent at the input, the NF of the parametric amplification process (see equation 2.20) simplifies to the following relation

$$NF_{s,PIA} = \frac{|\mu|^2 + |\nu|^2}{|\mu|^2} = \frac{2G_{PIA} - 1}{G_{PIA}} = 2 - \frac{1}{G_{PIA}} \tag{2.21}$$

which is the well known $3\ dB$ NF limit of phase insensitive amplification process. However for the case of phase sensitive amplification, where both the signal and idler waves are present at the input, the NF relation (see 2.20) takes the following form

$$NF_{s,PSA} = \frac{|\mu|^2 + |\nu|^2}{|\mu + \nu e^{j\phi}|^2} \tag{2.22}$$

assuming equal signal and idler powers at the input $|B_{s,in}|^2 = |B_{i,in}|^2$, where $\phi = \phi_s + \phi_i - \phi_{p1} - \phi_{p2}$. This implies that when the signal undergoes maximum phase sensitive gain ($\phi = 0$), the NF associated with the PSA of the signal turns out to be

$$NF_{s,PSA} = \frac{|\mu|^2 + |\nu|^2}{|\mu + \nu|^2} \approx \frac{2\mu^2}{4\mu^2} \equiv \frac{1}{2} \tag{2.23}$$

The noise figure of $-3\ dB$ for PSA is obtained by considering only signal power at the input. However, the noise figure of $0\ dB$ is obtained, if both signal and idler powers are considered at the input, in the high gain regime of phase sensitive amplification of the input signal. It is impossible to achieve this $0\ dB$ NF in case of PIA and erbium doped fiber amplifiers. In PSA, the coherent addition of phase locked signal and idler waves provides us with the advantage of $6\ dB$ improvement in the noise figure when compared to PIA process.

2.3 Parametric amplification with degenerate pump

The rest of the discussion in this chapter is focused on the parametric amplification using degenerate pump (see Fig. 2.1(a)). The transfer matrix K assumes the following

form in the degenerate pump case

$$K = \begin{bmatrix} \mu & \nu \\ \nu^* & \mu \end{bmatrix} = \begin{bmatrix} cosh(gz) + j\frac{\kappa}{g}sinh(gz) & j\frac{\gamma P_p}{g}sinh(gz) \\ -j\frac{\gamma P_p}{g}sinh(gz) & cosh(gz) - j\frac{\kappa}{g}sinh(gz) \end{bmatrix} \tag{2.24}$$

where P_p represents the pump power, $\Delta\beta = \beta_s + \beta_i - 2\beta_p$ denotes the dispersive phase mismatch, $2\kappa = 2\gamma P_p + \Delta\beta$ represents the net phase mismatch and $g = \sqrt{(\gamma P_p)^2 - \kappa^2}$ is the parametric gain coefficient. However, the gain and noise characteristics that have been inferred from the properties of the transfer matrix K in the previous section (see Section 2.2) holds good, as the transfer matrix (K) assumes the same form in the degenerate pump case as well. The gain experienced by the signal in parametric amplification process is primarily contingent on dispersion, nonlinearity of the medium, length of optical interaction and pump power which are analysed in this section.

2.3.1 PIA - Dependence on dispersion, nonlinearity, pump power

In the absence of idler, the gain experienced by the signal (G_{PIA}) and the idler conversion efficiency (η_{PIA}) in the PIA process are obtained from equation 2.24 as

$$\begin{aligned} G_{PIA} &= \frac{P_{sig}(z)}{P_{sig}(0)} = cosh(gz)^2 + \left(\frac{\kappa}{g}sinh(gz)\right)^2 \\ \eta_{PIA} &= \frac{P_{idler}(z)}{P_{sig}(0)} = \left(\frac{\gamma P_p}{g}sinh(gz)\right)^2 \end{aligned} \tag{2.25}$$

The signal gain and the idler conversion efficiency are maximised when parametric gain coefficient (g) is maximised. The parametric gain coefficient as expressed in equation 2.24 attains the maxima when the net phase mismatch is zero ($\kappa = 0$). The net phase mismatch in PIA process can be expressed by the following relation

$$2\kappa = \gamma P_p + \beta_2(\omega_s - \omega_p)^2 \tag{2.26}$$

where β_2 is the second order Taylor series coefficient of β expressed around ω_p and ω_p, ω_s represents the pump and signal frequencies respectively. It can be seen that β_2

should be negative (anomalous dispersion : $D > 0$) to attain $\kappa = 0$ in PIA process using degenerate pumps, which will result in maximum gain. We proceed to estimate G_{PIA} and η_{PIA} for HNLF of varying properties and these results are plotted as a function of signal detuning ($\Delta\lambda = \lambda_s - \lambda_p$) in this section. The results in this section hold good for the range of input signal powers that satisfy the undepleted pump approximation.

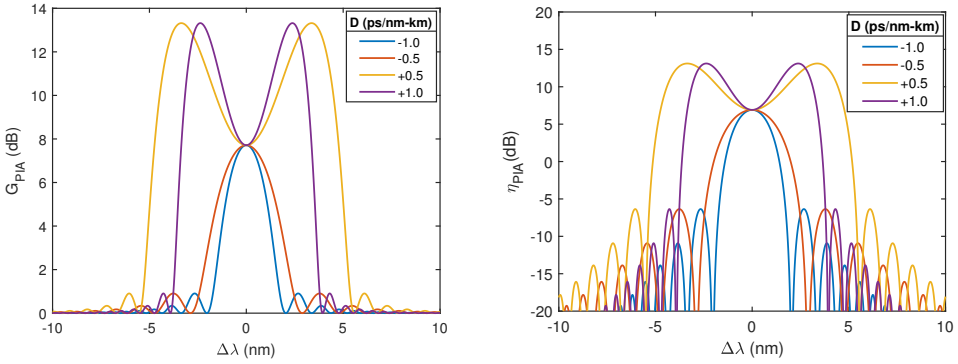

(a) (b)

Figure 2.2: Dependence of PIA (a) signal gain (b) idler conversion efficiency spectra on dispersion; $P_p = 23\ dBm$, $\gamma = 11.1\ W^{-1}km^{-1}$, $L = 1\ km$

The signal gain and idler conversion efficiency are plotted as a function of signal detuning for different values of dispersion parameter in Figure 2.2 for $P_p = 23\ dBm$, $\gamma = 11.1\ W^{-1}km^{-1}$, $L = 1\ km$. It can be noted that the gain attains the maximum in the anomalous dispersion regime as expected. Also, the gain bandwidth is higher when D approaches zero in the anomalous dispersion regime and it can be attributed to the fact that the dispersive phase mismatch is minimised when D approaches zero. Additionally, the gain flatness depends on the dispersion parameter of HNLF. Ideally, a flat gain can be achieved when β is not a function of wavelength in the interested wavelength range.

The signal gain and idler conversion efficiency in PIA process are plotted as a function of signal detuning for different values of nonlinear parameter (γ) in Figure 2.3 for $P_p = 23\ dBm$, $D = 1\ ps/nm - km$, $L = 1\ km$. It is observed that the signal gain and its bandwidth increases with the increase in nonlinear parameter as expected.

Similarly the dependence of signal gain and idler conversion efficiency on pump power in PIA process is plotted in Figure 2.4. And the increase in pump power increases the signal gain and bandwidth of PIA process similar to that of nonlinear parameter. The noise figure associated with the phase insensitive amplification process is clearly

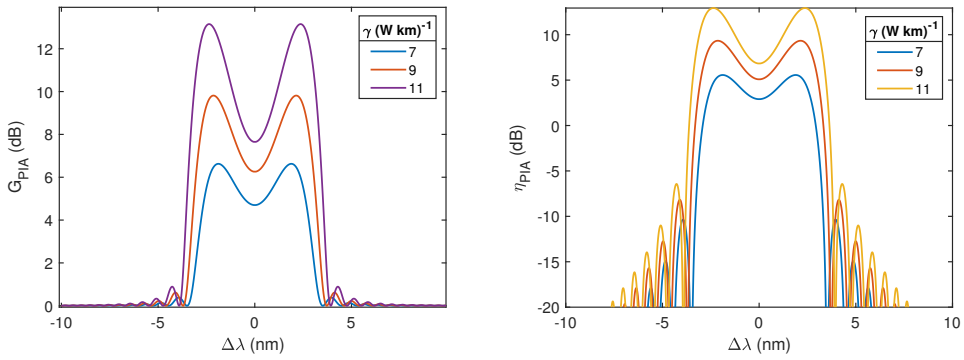

(a) (b)

Figure 2.3: Dependence of PIA (a) signal gain (b) idler conversion efficiency spectra on nonlinearity; $P_p = 23\ dBm$, $D = 1\ ps/nm - km$, $L = 1\ km$

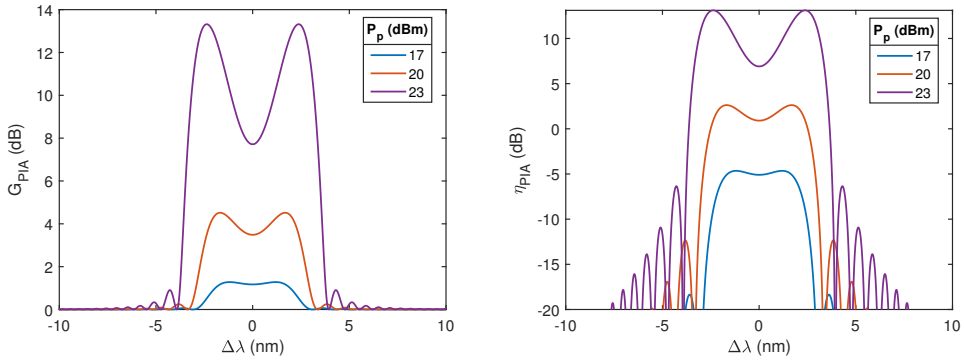

(a) (b)

Figure 2.4: Dependence of PIA (a) signal gain (b) idler conversion efficiency spectra on pump power; $\gamma = 11.1\ W^{-1}km^{-1}$, $D = 1\ ps/nm - km$, $L = 1\ km$

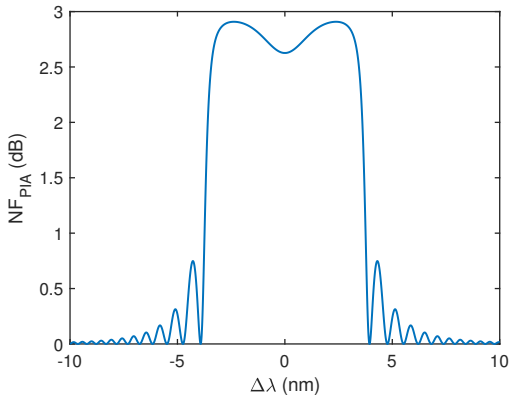

Figure 2.5: NF as a function of signal detuning in PIA process; $P_p = 23\ dBm$ $\gamma = 11.1\ W^{-1}km^{-1}$, $D = 1\ ps/nm - km$, $L = 1\ km$

explained in Section 2.2.3 and is plotted in the figure below (see Figure 2.5). Also, the noise figure approaches the $3\ dB$ limit when the signal gain is maximum. The noise figure in PIA process will be $3\ dB$ when $G_{PIA} >> 1$. It can be observed that the noise figure is lesser than $3\ dB$ in the low gain regime. This can be to the attributed to the fact

that there is no significant amplified quantum noise addition in the lower gain regime.

2.3.2 PSA - Gain and noise figure

In the presence of both signal and idler waves at the input, the signal experiences phase sensitive gain due to the coherent superposition of signal and idler waves. The maximum phase sensitive gain that the signal can attain at different detunings in PSA process is plotted in Figure 2.6 for equal signal and idler powers at the input. It can be noted that the maximum gain that the signal can attain in PSA process is almost $6\ dB$ more than that of PIA process as explained in the previous section (see Section 2.2.2).

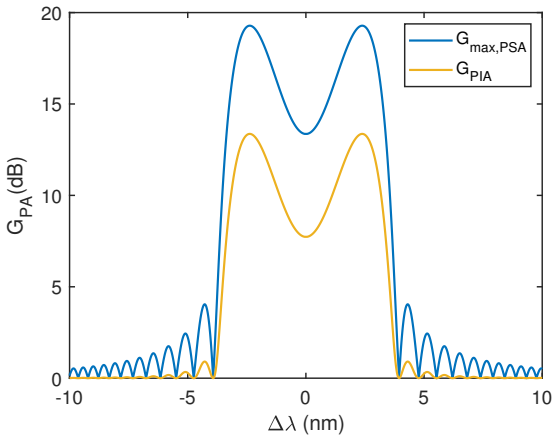

Figure 2.6: Maximum signal in PSA process for equal signal and idler powers at the input; $P_p = 23\ dBm\ \gamma = 11.1\ W^{-1}km^{-1}$, $D = 1\ ps/nm - km$, $L = 1\ km$

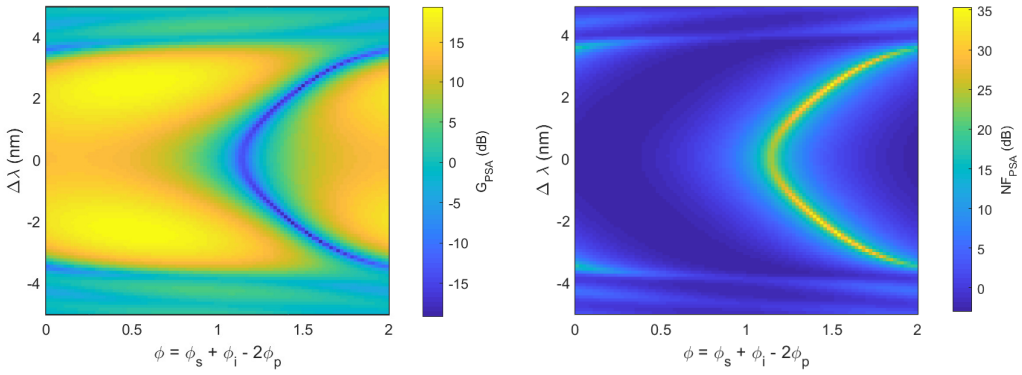

(a) (b)

Figure 2.7: (a) Signal gain and (b) noise figure in PSA process as a function of input phase relation and signal detuning; $P_p = 23\ dBm\ \gamma = 11.1\ W^{-1}km^{-1}$, $D = 1\ ps/nm - km$, $L = 1\ km$

However, the gain and noise figure experienced by the signal in PSA is heavily

dependent on the input phase relation $\phi = \phi_s + \phi_i - 2\phi_p$ and the signal detuning ($\Delta\lambda = \lambda_s - \lambda_p$) from the pump and this dependence is plotted in Figure 2.7 for the case of equal signal and idler powers at the input. It can be observed that the maximum gain that is achievable at a specific wavelength in PSA process occurs at different input phase relations for different signal detuning. It can be attributed to the fact that the parametric gain coefficient g depends on $\phi = \phi_s + \phi_i - 2\phi_p + \angle\mu - \angle\nu$ (see Section 2.2.2) which brings in the dependence with respect to signal detuning. Also, it can be observed in Figure 2.7a that the signal undergoes amplification or attenuation depending on the phase relation between the pump, signal and idler waves as explained in the previous section (see Section 2.2.2). Also, the noise figure in the high gain regime can be observed as $-3dB$ which is an improvement of $6\ dB$ with respect to that of PIA. The signal gain and the associated noise figure at particular input phase relations are further plotted in Figure 2.8. However for a given phase relation, the maximum gain and minimum NF occurs at slightly different detunings. This can be attributed to the fact that noise at signal and idler wavelengths are not correlated whereas the signal and idler waves are correlated with each other, resulting in different detuning performances for added noise and the signal gain, as can be seen from equations 2.18 and 2.22.

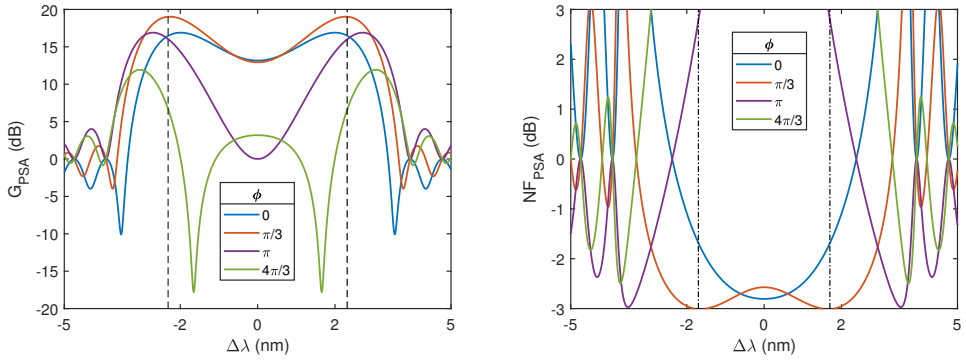

(a) (b)

Figure 2.8: Dependence of PSA (a) signal gain and (b) noise figure for different input phase relations, dashed line: maximum gain, dash-dotted line: minimum NF; $P_p = 23\ dBm\ \gamma = 11.1\ W^{-1}km^{-1}$, $D = 1\ ps/nm - km$, $L = 1\ km$

Based on the discussions held in this section (Section 2.3), it can be concluded that the gain can be increased with the increase in the pump power for a HNLF of given parameters. However, the maximum power that can be launched into the fiber is severely limited by stimulated Brillouin scattering, which is a major drawback in fiber based parametric amplifiers.

2.4 Stimulated Brillouin Scattering in optical fibers

Stimulated Brillouin Scattering (SBS) is a nonlinear interaction process between the pump wave and the back-propagating signal wave through an acoustic wave at power levels much lesser than of the requirement of parametric amplification process in optical fibers. After reaching the threshold condition for the SBS process, the majority of the pump power is transferred to the back-propagating signal wave which in-turn limits the pump power that can be launched into the fiber for parametric amplification process. The Brillouin gain $g_B(\Omega)$ has a Lorentzian spectrum of the below mentioned form (Agrawal (2000))

$$g_B(\Omega) = g_p \frac{\left(\frac{\Gamma_B}{2}\right)^2}{\left(\Omega - \Omega_B\right)^2 + \left(\frac{\Gamma_B}{2}\right)^2} \tag{2.27}$$

where the phonon lifetime (T_B) is related to Γ_B as $T_B = \frac{1}{\Gamma_B} = 10\ ns$ and Ω_B refers to the Brillouin shift in optical fibers. The peak of the spectrum occurs at $\Omega = \Omega_B$ and the full width at half maximum of the gain spectrum is related to Γ_B as $\Delta\nu_B = \frac{\Gamma_B}{2\pi}$ which is around $30\ MHz$ for silica fibers. The SBS threshold is found to occur at a critical power level which is given by the following empirical relation (Smith (1972)) as

$$\frac{g_B P_{th} L_{eff}}{A_{eff}} \approx 21 \tag{2.28}$$

where P_{th} refers to the SBS threshold in optical fibers, A_{eff} refers to the effective modal area and L_{eff} refers to effective interaction length. However, the SBS threshold increases considerably if the spectral width $\Delta\nu_p$ of the pump exceeds $\Delta\nu_B$ as a consequence of decrease in the Brillouin gain parameter g_B and this increase in SBS threshold is characterised by the factor $\left(1 + \frac{\Delta\nu_p}{\Delta\nu_B}\right)$ (Agrawal (2000)). The SBS threshold for typical HNLF fibers of $1\ km$ length is around $10\ dBm$ that limits the pump power that can be launched into HNLF for parametric amplification process. However, a minimum pump power of $20\ dBm$ is required to attain a PIA gain of $\approx 5\ dB$ in HNLF.

2.4.1 SBS mitigation strategies

The SBS mitigation strategies are either focused on broadening the Brillouin gain spectrum and thus decreasing the peak gain or increasing the pump linewidth to minimise

the spectral overlap which limits the gain experienced by the back-propagating signal.

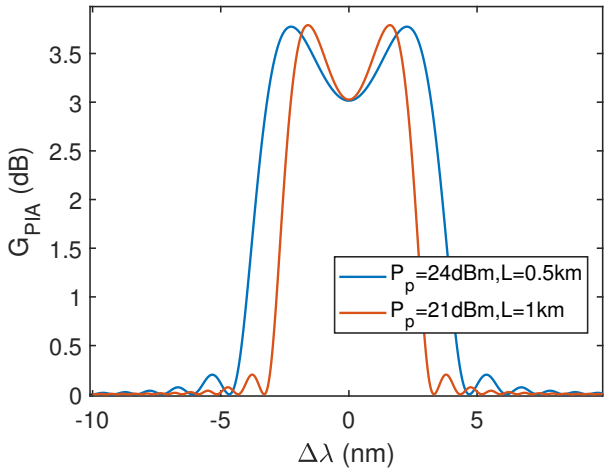

Figure 2.9: PIA signal gain spectrum of "SPINE" HNLF

The typical methods to broaden the Brillouin gain spectrum to increase the SBS threshold include: introduce temperature gradients along the fiber (Hansryd *et al.* (2001)), introducing strain gradients along the fiber (Engelbrecht *et al.* (2009), Boggio *et al.* (2005)) and changing the dopant concentration along the length of the fiber (Shiraki *et al.* (1996)). The change in dopant concentration, strain, temperature along the length of the fiber introduces the modulation of refractive index of the material along the length of the fiber that results in a continuous change of Brillouin shift (Ω_B) along the fiber. This continuous change of Brillouin shift along the length of the fiber results in a significant broadening of Brillouin gain spectrum increasing the SBS threshold of the optical fibers. The "SPINE" (stable phase matching for improved nonlinear efficiency) HNLF, manufactured by OFS, has the following the characteristics: $\gamma = 9.3\, W^{-1}km^{-1}$, $D = 1\ ps/nm - km$, dispersion slope of $0.071\ ps/nm^2km$ and it exhibits a significantly higher SBS threshold of $24\ dBm$ (Labidi *et al.* (2018)). The PIA gain that can be attained from the above mentioned "SPINE" HNLF without any active SBS suppression techniques is plotted in Figure 2.9. It is clearly impossible to attain the similar performance in normal HNLF without any active SBS mitigation strategies as the SBS threshold limits the pump power that can be launched to be around $\approx 10\ dBm$. These passive methods clearly demonstrate a special advantage of requiring no additional optical components/ setup to mitigate SBS in parametric amplification experiments. Also, these methods do not affect the properties of the incoming signal as compared to that of the method of increasing the pump linewidth to increase the SBS threshold. However, these passive methods require special fabrication of fibers and longitudinal temperature

and strain variation methods require sophisticated setup to vary temperature and strain that poses a challenge of scalability of such systems.

One of the active methods that employs the strategy of increasing the pump linewidth to increase the SBS threshold is to phase modulate the pump wave using RF tones or RF noise source (Anderson *et al.* (2014)). This approach of active suppression of SBS in HNLF does not face any fabrication challenges, but faces other significant challenges which sets the discussion for next chapter.

CHAPTER 3

Experimental Demonstration of Parametric Amplification in HNLF

One of the main criteria to demonstrate parametric amplification in HNLF is to launch several hundred milliwatts of pump power to provide sufficient gain to the signal. However, the launch pump power is limited by the SBS threshold as seen in the previous chapter (see Section 2.4). Hence, the successful demonstration of PA in HNLF should employ one of either passive or active SBS suppression strategies. Given the challenge of scalability of passive SBS suppression techniques, it is highly imperative to experiment active SBS suppression methodologies. A commonly used active method in FOPA systems is the phase modulation of pump laser for linewidth broadening because of its easy implementation along with effective suppression of SBS.

3.1 SBS suppression using phase modulation of pump

Phase modulation of pump laser falls in the category of increasing the pump linewidth to minimize the overlap between the pump wave and SBS gain spectrum to increase the SBS threshold. The typical Brillouin spectrum of a single mode optical fiber is shown in Figure 3.1. It can be seen that the frequency shift is around $11\ GHz$ and with a FWHM of $\approx 30\ MHz$. Hence, it becomes essential to the broaden the linewidth of the pump beyond FWHM of Brillouin gain spectrum ($30\ MHz$) to suppress SBS in optical fibers.

The electric field of the pump wave can be described by the following expression

$$E_p(t) = E_0\, e^{j(\omega_p t + \phi)} \tag{3.1}$$

If the pump output is phase modulated using an RF signal of amplitude A_m and fre-

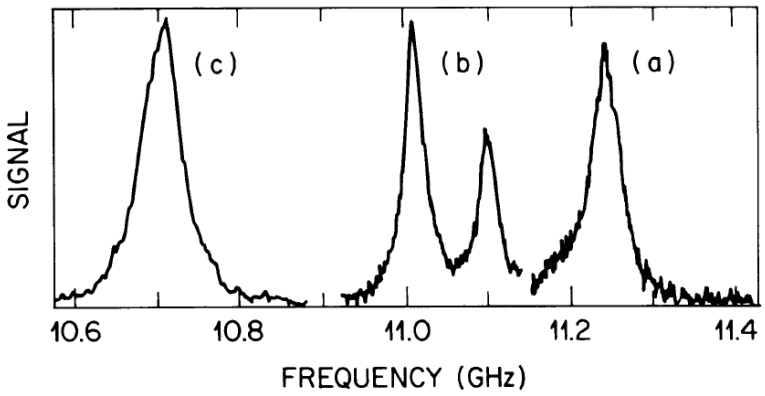

Figure 3.1: Brillouin gain spectra of three different single mode fibers versus frequency shift at $\lambda_p = 1550\ nm$ (a) silica core fiber (b) depressed cladding fiber (c) dispersion shifted fiber (Tkach *et al.* (1986))

quency v_m, the pump output at the phase modulator can be obtained as

$$\begin{aligned} E_{PM}(t) &= E_p(t)\ e^{j(A_m sin(2\pi v_m t))} \\ &= E_0\ e^{j(\omega_p t + \phi + A_m sin(2\pi v_m t))} \\ &= J_0(\beta_m)\ e^{j\omega_p t} + \sum_n A_m J_n(\beta_m)[\ e^{j(\omega_p + 2\pi n v_m)t} - e^{j(\omega_p - 2\pi n v_m)t}\ ] \end{aligned} \tag{3.2}$$

where $\beta_m = \frac{A_m}{v_m}$ and J_n is the Bessel function of the first kind with order m. Equation 3.2 demonstrates the broadening of the pump due to phase modulation using RF signal. The RF tones used should be more than that of the SBS gain FWHM ($30\ MHz$) to minimise the overlap. The phase modulated spectra of pump using an RF of signal of $100\ MHz$ frequency with amplitude levels of $0.5V_\pi$ and $2V_\pi$ are plotted in Figure 3.2. V_π is the half-wave voltage of the electro-optic phase modulator.

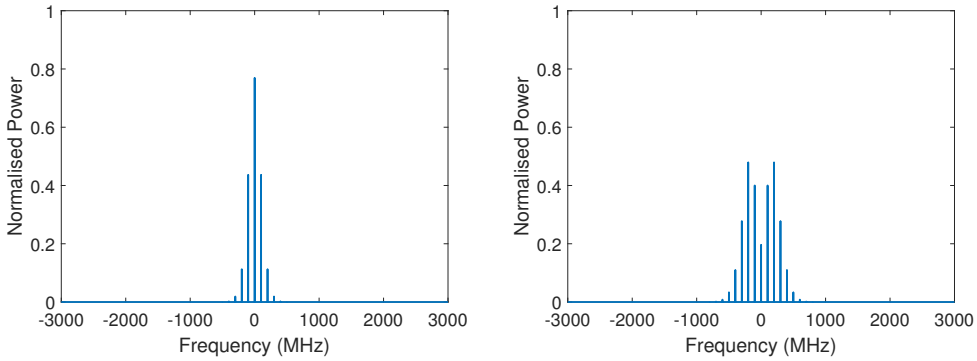

(a) (b)

Figure 3.2: Phase modulated spectra of pump with RF signal of $v_m = 100\ MHz$ and amplitude (a) $A_m = 0.5V_\pi$ (b) $A_m = 2V_\pi$

It can be seen that the broadening of the pump increases with the drive voltage of

the phase modulator. The broadening of the pump also varies with the usage of multiple sinusoidal tones rather than a single tone which is illustrated in Figure 3.3.

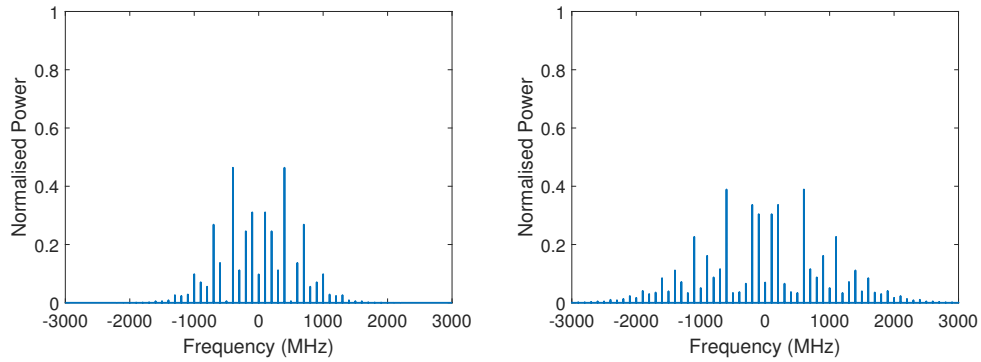

(a) (b)

Figure 3.3: Phase modulated spectra of pump with RF signal of $A_m = 2V_\pi$ and frequency tones (a) $100\ MHz$ & $300\ MHz$ (b) $100\ MHz$, $300\ MHz$ & $500\ MHz$

It can be seen that the pump spectra significantly broadens with the number of sinusoidal tones used for the same drive voltage level. If the phase modulator is driven at $2V_\pi$ with multiple sinusoidal RF tones of frequencies $100\ MHz, 300\ MHz$ and $500\ MHz$, the broadened pump linewidth can be noted to be in the order of several hundred MHz, which is significantly high compared to SBS gain FWHM of $30\ MHz$. Hence, it can be inferred that the phase modulator should be driven at a higher voltage with a combination of multiple sinusoidal tones to sufficiently broaden the pump linewidth beyond SBS gain FWHM to achieve effective suppression of SBS in optical fibers.

3.1.1 Experimental results and discussions

The experimental setup for SBS suppression using phase modulation and SBS threshold measurement is shown in Figure 3.4. The pump laser operating at a wavelength of $\lambda_p = 1546.4\ nm$ is used in the experiment. The pump is modulated using an electro-optic phase modulator whose half-wave voltage (V_π) is around $6\ V$. The pump wave is passed through the polarization controller to the phase modulator to ensure maximum power at the output of phase modulator. The pump power is further amplified using an Erbium doped fiber amplifier (EDFA) and successively passed through an optical band pass filter (BPF) of $0.1\ nm$ bandwidth to filter out the excessive out-of-band amplified spontaneous emission (ASE) noise from EDFA. The output from the EDFA is passed

to the HNLF through a circulator to prevent the back scattered power from damaging the optical components. The back scattered power is measured using a power meter at port-3 of the circulator. Also, the power output at the HNLF is measured using a power meter at the HNLF end.

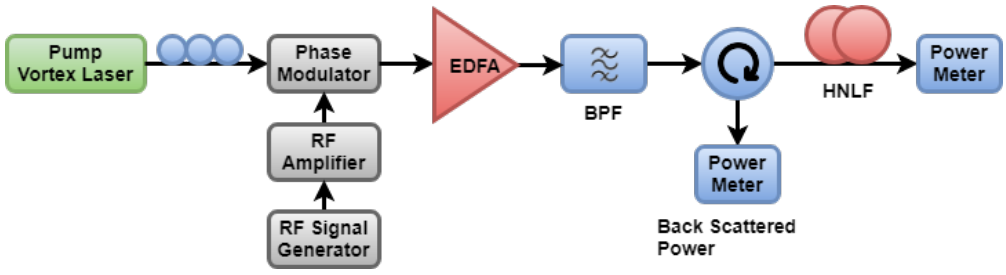

Figure 3.4: Experimental setup for SBS suppression using phase modulation and threshold measurement

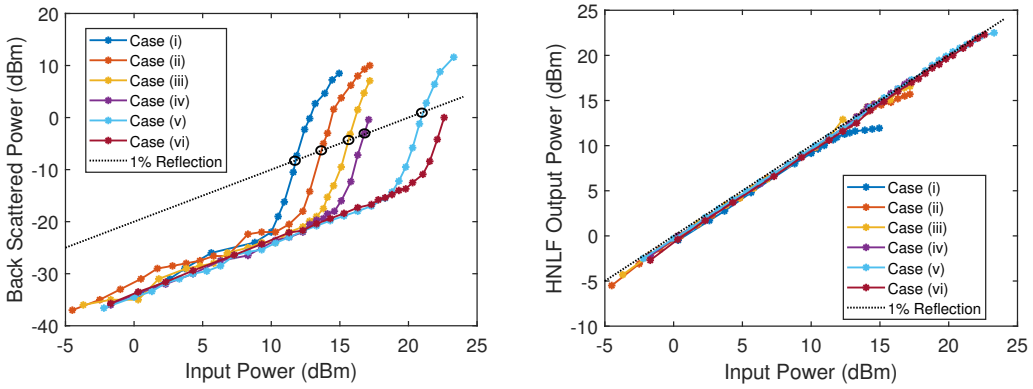

(a) (b)

Figure 3.5: (a) Back scattered power (b) output power from HNLF for different phase modulation inputs; black circles indicate 1% reflection, different cases are listed in the table below (see Table.3.1)

Table 3.1: SBS threshold for different RF signal inputs to phase modulator

Case	RF power (dBm)	Frequency content (MHz)	Measured SBS threshold
(i)	-	-	11.7
(ii)	18	100	13.6
(iii)	18	100	15.6
(iv)	18	100, 310	16.8
(v)	23	100, 310	21
(vi)	23	100, 310, 550	>22.5

To study the effect of phase modulation of pump using different RF tones and drive voltage levels, the set of RF signals that are chosen as input to the phase modulator are mentioned in Table.3.1. Here in Table.3.1, case (i) represents no external phase modulation being applied to the pump. The input pump power to EDFA is varied to

tune the power levels being input into HNLF. The properties of HNLF used in the experiment are: $\gamma = 11.1\ W^{-1}km^{-1}$, $D = -0.65\ ps/nm.km$ and $L = 1\ km$. The back scattered power from HNLF and the power at HNLF output for all the cases listed in Table.3.1 are plotted in Figure 3.5a and Figure 3.5b respectively as a function of input power level. SBS threshold is defined as the input power at which 1% of the input power reflects back from the HNLF. The measured SBS threshold for different phase modulated inputs are also listed in Table.3.1. It can be seen that the SBS threshold for pump without any external phase modulation is around $\approx 11.7\ dBm$ for HNLF. Also, the SBS threshold increases with the drive voltage and multiple frequency tones as expected from the theory. It is observed that $\approx 23\ dBm$ of pump power can be launched into HNLF without any significant back scattering by choosing the RF signal input mentioned in case (vi) of Table.3.1.

3.2 Degenerate pump PIA experimental results and discussions

The experimental setup for demonstrating PIA in HNLF is shown in Figure 3.6. The setup is similar to that of the SBS suppression setup (See Figure 3.4) except for the signal laser which is coupled into HNLF along with pump using a 99:1 coupler. The polarization controller is used in the signal arm to align the polarization of pump and signal to ensure maximum PIA gain. The wavelength of the signal laser is tuned to obtain the PIA gain spectrum. The RF signal input applied to the phase modulator corresponds to that of case (vi) listed in Table.3.1 which allows $\approx 23\ dBm$ of pump launch power without any significant back scattering in HNLF. The pump and signal powers launched into HNLF are maintained at $22\ dBm$ and $-11\ dBm$ respectively.

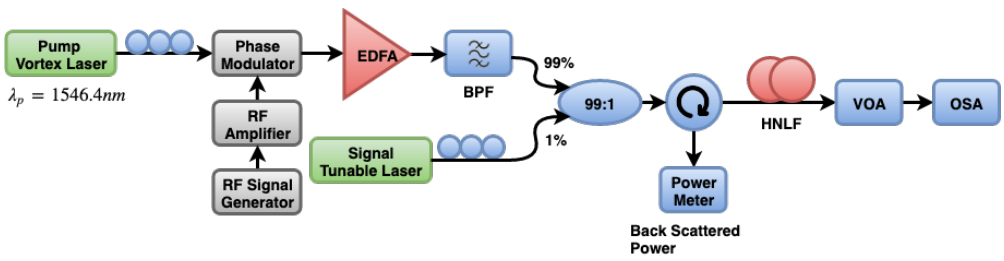

Figure 3.6: Experimental setup for degenerate pump PIA in HNLF

The signal gain and idler conversion efficiency are measured from observing the

power levels at the output of HNLF at signal and idler wavelengths using optical spectrum analyser (OSA). The recorded spectrum at the output of HNLF using OSA for the signal wavelength of $1545\ nm$ is shown in Figure 3.7 .The signal gain is measured by comparing the power levels at signal wavelength at the output of HNLF in the presence and absence of the pump. The experimentally obtained signal gain (G_{PIA}) and idler conversion efficiency spectra (η_{PIA}) are plotted in Figure 3.8a and Figure 3.8b respectively. It can be observed that the experimentally obtained G_{PIA} and η_{PIA} are in excellent matching with the theoretically analysis.

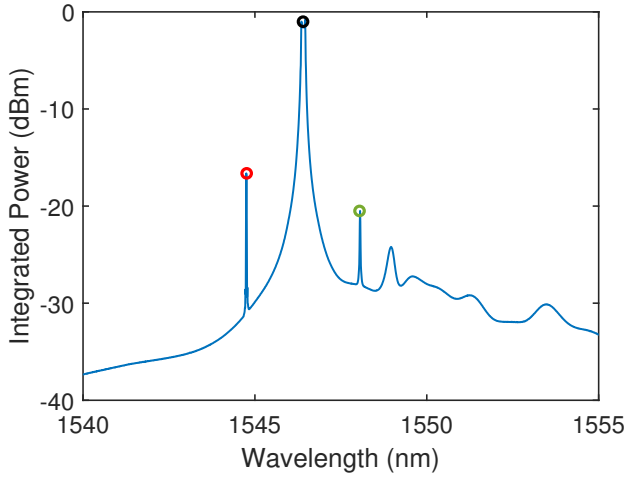

Figure 3.7: Normalised signal spectrum at the output of HNLF for $\lambda_p = 1546.4\ nm$, $\lambda_s = 1545\ nm$; black circle - pump, red circle - signal, green circle - idler

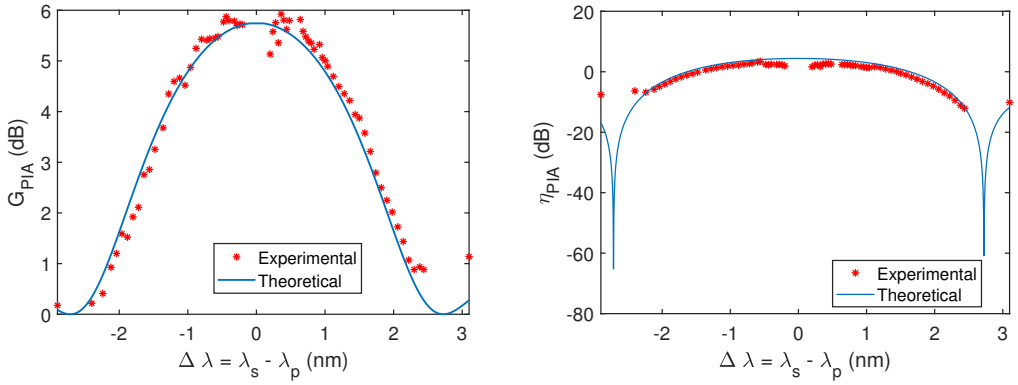

(a) (b)

Figure 3.8: PIA (a) signal (b) idler conversion efficiency as a function of signal detuning for degenerate pump case

Since we are operating in the normal dispersion regime, the maximum signal gain occurs when signal wavelength is closer to pump wavelength as further detuning results in increased phase mismatch as both dispersive phase mismatch and nonlinear phase mismatch add to each other. A maximum signal gain of $6\ dB$ and conversion efficiency

of $0\ dB$ is experimentally demonstrated using a pump power of $22\ dBm$ and active SBS suppression using phase modulation of pump.

To demonstrate the PIA amplification of QPSK data and also analyse the BER of the amplified signal, the IQ transmitter laser is operated at $1547.4\ nm$ and is modulated with $21\ GBd$ QPSK data generated using an arbitrary wave form generator (AWG). The modulated signal is then coupled into HNLF along with the pump using a 99:1 coupler. The signal attained a PIA gain of $3\ dB$ similar to that of continuous wave case as expected. The constellation diagram of the amplified signal in PIA process using degenerate pump is shown in Figure 3.9. It can be observed from the constellation

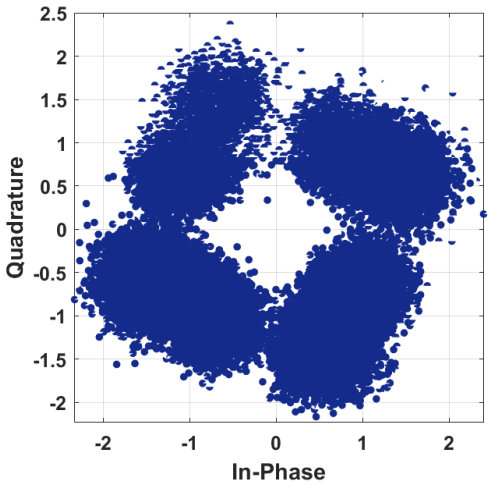

Figure 3.9: Constellation diagram of $21\ GBd$ QPSK signal amplified in PIA process using degenerate pump

diagram that the signal is highly corrupted in phase and the signal is observed to have a BER of 10^{-2} after processing using DSP algorithms for an input OSNR of around $33\ dB$ which is unacceptable in communication standards. The corruption in phase of the amplified signal can be attributed to the phase modulation of the pump using RF signals in the order of several MHz for increasing the SBS threshold.

3.3 Dual pump PIA using counter phase modulation for SBS suppression

As seen in the previous section (see Section 3.2), the phase modulation of pump for increasing the SBS threshold severely affects the phase of the amplified signal which

worsens the BER performance in phase shift keying signalling scheme. However, its imperative to have phase modulation of pump to broaden the pump linewidth for active SBS suppression. Hence, it is required to come up with a scheme which cancels the effect of phase modulation of pump on the signal and idler waves. If the powers of the two pumps are P_{p1} and P_{p2} in dual pump PIA , the phase of the amplified signal and the idler generated is given by the following expression (Moro *et al.* (2010))

$$\begin{aligned}\phi_s(t,L) =&\phi_s(t,0) + tan^{-1}\left(\frac{\kappa(t)sinh[g(t)L]}{2g(t)cosh[g(t)L]}\right)\\ &+\frac{\gamma}{2}\left|\sqrt{P_{p1}}+n_1(t)\right|^2 L+\frac{\gamma}{2}\left|\sqrt{P_{p2}}+n_2(t)\right|^2 L+\frac{\Delta\beta(t)L}{2}+\Delta\phi_{s,AQN}\\ \phi_i(t,L) =&[\phi_{p1}(t,0)+\phi_{mod1,p1}+\phi_{p2}(t,0)+\phi_{mod2,p2}-\phi_s(t,0)]+\frac{\pi}{2}\\ &+\frac{\gamma}{2}\left|\sqrt{P_{p1}}+n_1(t)\right|^2 L+\frac{\gamma}{2}\left|\sqrt{P_{p2}}+n_2(t)\right|^2 L+\frac{\Delta\beta(t)L}{2}+\Delta\phi_{i,AQN}\end{aligned} \tag{3.3}$$

The second term in the expression is a consequence of μ and ν that are associated with the signal gain and idler conversion efficiency respectively. The third and fourth terms in the expressions are the consequences of SPM and XPM in nonlinear medium. The amplitude fluctuations present in the pumps translate as phase noise in the signal and the idler. Here, n_1 and n_2 refer to the amplitude noise present in the pumps. The fifth term refers to the phase acquired by the signal and the idler due to the dispersive nature of the medium, which is given by

$$\Delta\beta(t)=\frac{\beta_2}{2}\left[2(\omega_s-\omega_0)^2-\left(\omega_{p1}+\frac{d\phi_{mod1,p1}}{dt}-\omega_0\right)^2-\left(\omega_{p2}+\frac{d\phi_{mod2,p2}}{dt}-\omega_0\right)^2\right] \tag{3.4}$$

where $\omega_0=\frac{\omega_{p1}+\omega_{p2}}{2}$ refers to the center frequency of the system. The final term AQN refers to the quantum noise in the system. $\phi_{mod,p1}$ and $\phi_{mod,p2}$ correspond to the phase modulation applied to pump (1) and pump (2) respectively. This illustrates the noise transfer happening to the idler wave because of the modulation of pumps to increase the SBS threshold. However, the signal phase also gets affected due to pump phase modulation due to the change in the pump frequency, which results in a change of the phase acquired by the signal due to dispersion. Hence, it is clear that the idler phase is affected severely compared to that of the signal phase because of its associated

broadening. In order to mitigate the idler broadening due to phase modulation of pump, the required relation between the applied RF inputs to phase modulators of the pumps is given by

$$\begin{aligned} \phi_{mod,p1} &= -\phi_{mod,p2} \\ V_{RF,p1} &= -V_{RF,p2} \end{aligned} \tag{3.5}$$

where $V_{RF,p1}$ and $V_{RF,p2}$ are the RF signal inputs to the phase modulators present in the arms of pump (1) and pump (2) respectively. In this case, the effect due to phase modulation applied to pump (1) and pump (2) on idler phase cancel each other. Hence, it is required to implement dual pump configuration with counter phase modulation to demonstrate parametric amplification and noise free phase conjugation of QPSK signal (Hu *et al.* (2015), Yaman *et al.* (2005)).

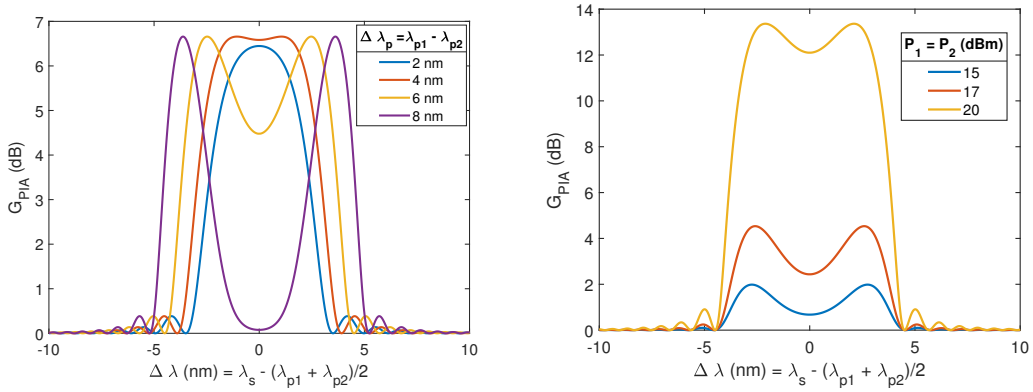

(a) (b)

Figure 3.10: Dual pump configuration PIA signal gain spectra for (a) different pump separation and $P_{p1} = P_{p2} = 18\ dBm$ (b) different pump power levels and $|\lambda_{p1} - \lambda_{p2}| = 6\ nm$

The PIA gain spectra for different separation of pump waves $\Delta\lambda_p = |\lambda_{p1} - \lambda_{p2}|$ at pump power levels of $P_{p1} = P_{p2} = 18\ dBm$ are obtained using analytical expressions presented in the previous chapter (see Section.2.2.2) and are plotted in Figure 3.10a. Similarly, the gain spectra for different pump power levels at a specific separation of $6\ nm$ between the pump waves are plotted in Figure 3.10b. The properties of HNLF are $\gamma = 11.1\ W^{-1}km^{-1}$, $D = -0.65\ ps/nm.km$ and $L = 1\ km$.

The analytical plots demonstrate the fact that the PIA signal gain spectra heavily depends on the pump separation in case of dual pump configuration. This can be attributed to the fact that the dispersive phase mismatch is contingent on pump separation.

3.3.1 Experimental results and discussions

The experimental setup to implement dual pump configuration with counter phase modulation is shown in Figure 3.11. The pumps wavelengths are chosen as $\lambda_{p1} = 1546.4\,nm$ and $\lambda_{p2} = 1552.52\,nm$. The RF signals from positive and negative terminals of the RF signal generator are fed to the identical phase modulators present in the pump arms. The RF power inputs to the phase modulators are $\approx 23\,dBm$. RF signals consists of three different sinusoidal tones: $100\,Mhz$, $310\,MHz$ and $550\,MHz$. $30\,dB$ EDFA is used in the tunable laser arm and $23\,dB$ FA-23 EDFA is used in the vortex laser arm. The pumps are then combined using a 50:50 coupler which is then combined along with the signal using a 99:1 coupler that is fed into HNLF for PIA through circulator to prevent the reflected power from damaging the optical components. At the input of HNLF, the powers of pumps $\lambda_{p1}(1546.4\,nm)$ and $\lambda_{p2}(1552.52\,nm)$ are $16.5\,dBm$ and $18.5\,dBm$ respectively. The signal power coupled into the HNLF after $99:1$ coupler is $\approx -10dBm$. The waveshaper is used to filter out the pump wavelengths and the signal powers and idler powers are measured in OSA to obtain signal gain and idler gain respectively. The signal wavelength is tuned from $1544\,nm$ to $1554\,nm$ in this experiment. The various polarization controllers are used to align the polarization of the signal and pump waves to ensure maximum signal gain in PIA process.

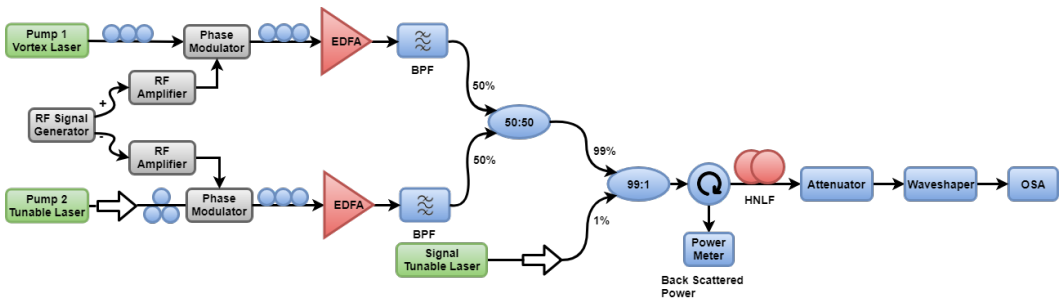

Figure 3.11: Experimental setup for dual pump PIA configuration with counter phase modulation

The spectrum at the output of HNLF for a specific detuning of signal ($\lambda_s = 1551\,nm$) is plotted in Figure 3.12. It can be seen that apart the idler that we are interested in ($\omega_{p1} + \omega_{p2} - \omega_s$), there are several other idlers present in the system. The signal gain in dual pump PIA in HNLF is plotted in Figure 3.13. As we saw in Figure 3.12, there are multiple other comparable idlers that are possible in this configuration. The idler conversion efficiencies of different such idlers are plotted in Figure 3.14 as a function of their corresponding wavelengths. Also, there are some idlers that are present in the

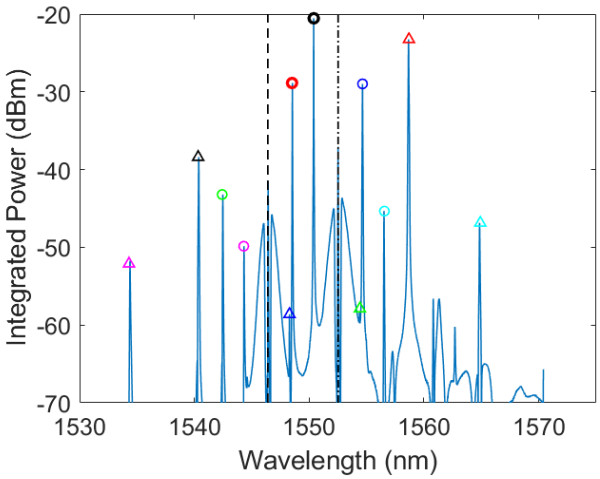

Figure 3.12: Spectrum at the output of HNLF; dashed line : ω_{p1}, dashed-dotted line : ω_{p2}, black circle : ω_s, red circle : $\omega_{p1} + \omega_{p2} - \omega_s$; circles indicate FWM products resulting from both signal and pump, triangles indicate FWM products resulting from two pumps

system, which are FWM products resulting from two different pumps present in the medium. The idler conversion efficiencies of such idlers are plotted in Figure 3.15. It can be seen the wavelengths of those idlers are invariant with respect to signal wavelengths as expected.

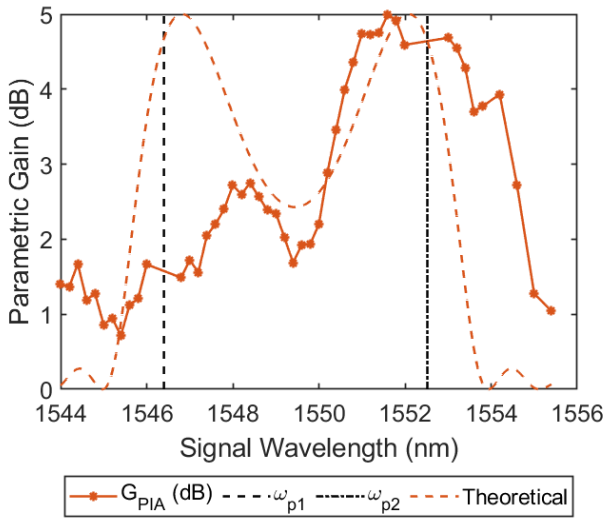

Figure 3.13: Dual pump PIA signal gain spectrum

From Figure 3.13, it can be seen that the signal gain has an asymmetric shape associated with it contrasting to that of the theoretical analysis. Also, the conversion efficiencies of different idlers are in the same order which is clearly not taken into account in the theoretical analysis. The asymmetry in the gain spectrum is possible when the following assumptions considered for the theoretical analysis are no more valid

(Steffensen *et al.* (2011))

- undepleted pump approximation
- interactions between $\omega_{p1}, \omega_{p2}, \omega_s, \omega_{p1}+\omega_{p2}-\omega_s$ are only considered in the system

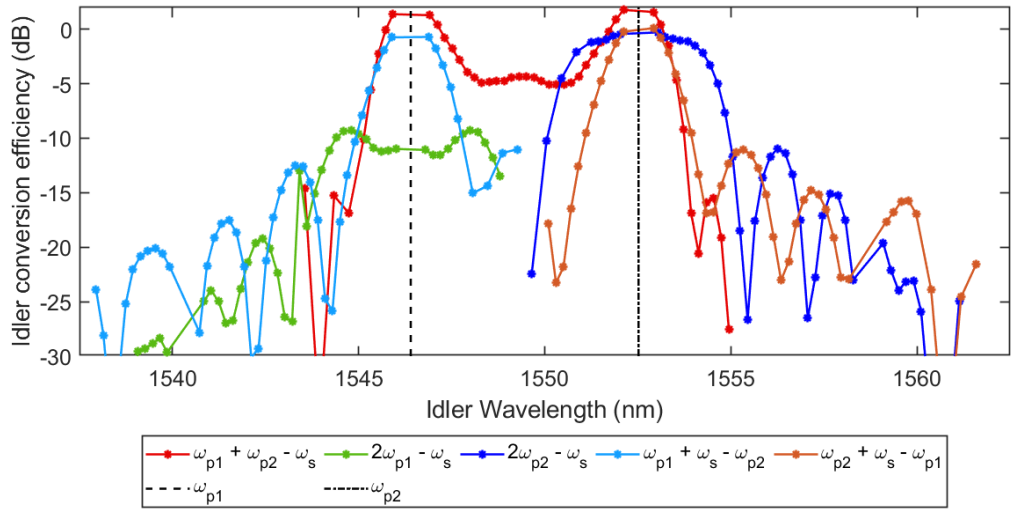

Figure 3.14: Dual pump PIA idler conversion efficiency of different possible idlers

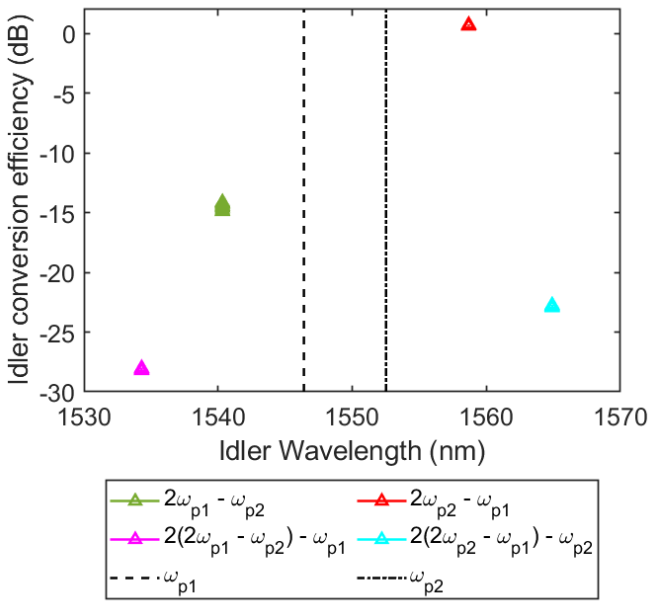

Figure 3.15: Dual pump PIA idler conversion efficiency of idlers dependent only on pumps

In order to demonstrate the PIA amplification of QPSK data and also analyse the BER of the amplified signal in dual pump configuration, the IQ transmitter laser is operated at $1551\ nm$ and is modulated with $21\ GBd$ QPSK data generated using an arbitrary wave form generator (AWG) with an OSNR of $\approx\ 33\ dB$. The OSNR of

Table 3.2: OSNR of signal and idler in dual pump PIA

Parameter	signal at HNLF input	signal at HNLF output	idler at HNLF output
OSNR	33 dB	30 dB	24 dB

the signal and the conjugate at the output of HNLF in dual pump PIA experiment are mentioned in Table.3.2. It can be noted that the noise figure associated with PIA in dual pump configuration is experimentally obtained as $3\ dB$. The gain experienced by the signal is $\approx 2.5\ dB$ with respect to peak power and found to have a BER of 0. The scatter plot of the received signal at the output of HNLF is shown in Figure 3.16. However, the idler is found to suffer from phase noise due to modulation even after implementation of dual pump configuration with counter phase modulation and observed to have a BER of $\approx 10^{-3}$. This can be attributed to the fact that cancellation of the phase noise due to RF signals is not achieved properly due to the potential delays between the RF signals.

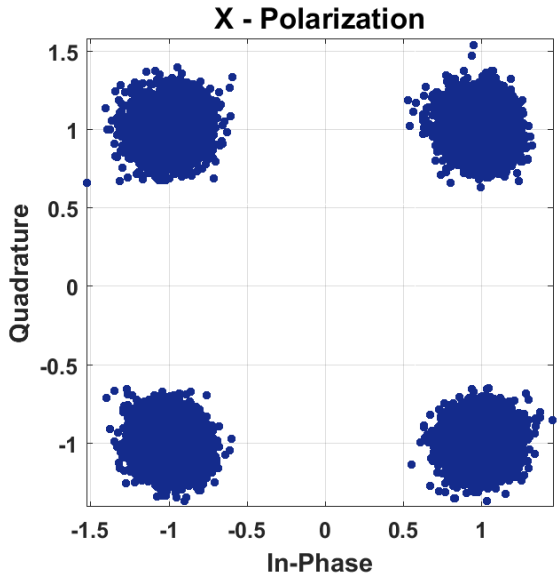

Figure 3.16: Scatter plot of signal at the output of HNLF; $OSNR = 31\ dB$, $BER = 0$, $EVM = 9.4\%$

It is evident from the discussions held in this chapter that it is essential to implement phase modulation of pump or any other passive technique for SBS suppression to demonstrate parametric amplification in HNLF. Also, it requires around $22\ dBm$ of pump power to achieve a parametric gain of $\approx 5\ dB$. Although, PA guarantees lesser noise figure, it requires us to look at other non-parametric media like semiconductor optical amplifiers as an alternative option because of the other difficulties and disadvantages associated with PA in HNLF.

CHAPTER 4

Semiconductor Optical Amplifiers

A Semiconductor optical amplifier (SOA) is a monolithic optoelectronic device that amplifies an input optical signal based on a semiconductor gain medium. ASE noise is a fundamental characteristic of the semiconductor gain media which results in a typically higher NF for the amplification process associated with SOA (Connelly (2007)). However, SOAs are attractive for their power efficiency, smaller footprint and potential for integration into silicon photonic platforms.

4.1 Four wave mixing in SOA

The phenomenon of four wave mixing in SOAs is a consequence of the physical processes that lead to population pulsations in semiconductor gain medium (Agrawal (1988)). In case of degenerate four wave mixing, the pump (frequency ω_p) and signal (frequency ω_s) waves create a beat frequency $\Omega = |\omega_s - \omega_p|$ in the medium and modulation of the carrier density at this beat frequency results in a formation of a gain grating and hence a corresponding refractive index grating at this beat frequency. This refractive index grating is responsible for the nonlinearities associated with semiconductor optical amplifiers. SOAs are amplifying nonlinear medium, whereas parametric amplifiers in HNLF, silicon based platforms are essentially of absorbing nature. As a consequence of this, the efficiency of the nonlinear processes are higher in SOA compared to that of other parametric amplifiers. In HNLF based fiber optic parametric amplifiers, pump power in the order of few hundred milliwatts is required to provide significant gain to the incoming signal. Whereas, a few milliwatts of pump power is enough to initiate nonlinearities in SOA because of its associated amplifying nature. ASE noise is absent in HNLF based parametric amplifiers as it does not involve any transitions between real energy levels. However, the requirement of phase modulation of pump to suppress SBS in HNLF makes the experimental setup quite complex in order to achieve viable amplification of phase modulated data with lesser phase corruption. Hence, the compact nature, power efficiency and easier realization of nonlinear processes make SOA

as a potential competent for optical signal processing applications as a nonlinear media. In SOAs, several nonlinear optical processing techniques like phase conjugation (Sobhanan *et al.* (2019), Sobhanan and Venkitesh (2018)), wavelength conversion (Nesset *et al.* (1998), Leuthold *et al.* (2000)) and phase quantization (Bottrill *et al.* (2015)) have been demonstrated in the past.

4.1.1 Modelling of SOA

The pulse propagation in SOAs can be explained by the following set of rate equations for the carrier density $N(z,t)$ and optical field $A(z,t)$ (Premaratne *et al.* (2008), Agrawal (1988)) as

$$\frac{\partial N(z,t)}{\partial t} = \frac{I}{qV} - \frac{N(z,t)}{\tau_s} - g(z,t)\frac{2\pi|A|^2}{h\omega} \tag{4.1}$$

where z and t denote space and time coordinates respectively, V corresponds to the volume of the active region, q is the electron charge, I is the injection current, ω is the operating frequency and τ_s represents the carrier lifetime. The gain coefficient $g(z,t)$ is defined as

$$g(z,t) = \Gamma a[N(z,t) - N_0] \tag{4.2}$$

where Γ describes the fraction of energy confined within the active region, a is the differential gain coefficient and N_o represents the carrier density at which the SOA becomes transparent. From equations 4.1 and 4.2, it can be obtained that

$$\frac{\partial g}{\partial t} = \frac{g_0 - g}{\tau_s} - \frac{g|A|^2}{E_{sat}} \tag{4.3}$$

where E_{sat} is the saturation energy of SOA, above which the SOA is heavily saturated and is expressed by the relation $E_{sat} = \frac{h\omega\sigma}{2\pi a}$ and σ is the modal cross-sectional area. g_0 represents the small signal gain coefficient and is given by the following expression as

$$g_0 = \Gamma a N_0 \left(\frac{I}{I_0} - 1\right) \tag{4.4}$$

where $I_0 = \frac{qVN_o}{\tau_s}$ denotes the current at which the SOA becomes transparent. $A = \sqrt{P}e^{j\phi}$ represents the optical field where P and ϕ correspond to the power and phase

of the optical field respectively. By shifting to the frame of reference that moves along with the pulse $\tau = t - \frac{z}{v_g}$, the equations through 4.1 and 4.3 can be summed up into following set of equations (Agrawal and Olsson (1989)).

$$\begin{aligned} \frac{\partial P}{\partial z} &= (g - \alpha_{int})P \\ \frac{\partial \phi}{\partial z} &= -\frac{1}{2}\alpha_L g \\ \frac{\partial g}{\partial \tau} &= \frac{g_0 - g}{\tau_s} - \frac{gP}{E_{sat}} \end{aligned} \tag{4.5}$$

where α_{int} represents the internal loss and α_L describes the linewidth enhancement factor. The solution for the set of equations listed in 4.5 is given by

$$\begin{aligned} P_{out}(\tau) &= P_{in}(\tau)e^{(h(\tau) - \alpha_{int}L)} \\ \phi_{out}(\tau) &= \phi_{in}(\tau) - \frac{1}{2}\alpha_L h(\tau) \end{aligned} \tag{4.6}$$

where $P_{in}(\tau)$ and $P_{out}(\tau)$ correspond to the input and output powers respectively and $\phi_{in}(\tau)$ and $\phi_{out}(\tau)$ correspond to the input and output phases respectively. The function $h(z, \tau)$ is the integrated gain at each point of the pulse profile and is given by the following equation

$$\begin{aligned} h(\tau) &= \int_o^L g(z, \tau)dz \\ \frac{dh}{d\tau} &= \frac{g_o L - h}{\tau_s} - \frac{P_{in}(\tau)}{E_{sat}}[e^h - 1] \end{aligned} \tag{4.7}$$

To include the effects of spectral hole burning and carrier heating as well, the parameters Δh_{shb} and Δh_{ch} are defined and included in the solution (Naimi *et al.* (2014)) as

$$\begin{aligned} \Delta h_{ch} &= \frac{-h}{h - \alpha_{int}L}(e^{(h - \alpha_{int}L)} - 1)P_{in}(\tau)\epsilon_{ch} \\ \Delta h_{shb} &= \frac{-h}{h - \alpha_{int}L}(e^{(h - \alpha_{int}L)} - 1)P_{in}(\tau)\epsilon_{shb} \\ P_{out}(\tau) &= P_{in}(\tau)e^{(h(\tau) + \Delta h_{ch} + \Delta h_{shb} - \alpha_{int}L)} \\ \phi_{out}(\tau) &= \phi_{in}(\tau) - \frac{1}{2}\alpha_L h(\tau) - \frac{1}{2}\alpha_{ch}\Delta h_{ch} \end{aligned} \tag{4.8}$$

where α_{ch} is the carrier heating gain phase coupling factor, ϵ_{ch} and ϵ_{shb} correspond to nonlinear gain suppression factor due to carrier heating and spectral hole burning respectively. The equations 4.6, 4.7 and 4.8 are numerically solved using predictor cor-

rector method (Wang *et al.* (2007)) to obtain the solutions and analyse the amplification process in SOA systematically.

4.1.2 Phase insensitive and phase sensitive gain

The parameters of SOA used in the simulation are listed in the following Table.4.1.

Table 4.1: SOA simulation parameters

Notation	Parameter	Value
$g_o L$	Gain parameter	10
$\alpha_{int} L$	Internal loss	4
τ_s	Carrier lifetime	25 ps
α_L	Linewidth enhancement factor	4
$P_{sat}(\frac{E_{sat}}{\tau_s})$	Saturation power	2 mW
ϵ_{ch}	Carrier heating nonlinear gain suppression factor	0.5 W^{-1}
ϵ_{shb}	Spectral hole burning nonlinear gain suppression factor	2 W^{-1}
α_{ch}	Carrier heating gain phase coupling factor	0.5

In order to study the phase insensitive amplification in degenerate configuration in SOA, a pump and a signal have been considered at the input with the idler being absent at the input of SOA. The pump wavelength is fixed at $\lambda_p = 1550\ nm$ and the signal wavelength is tuned to obtain the PIA gain spectra in SOA. The gain spectra and idler conversion efficiency spectra for a fixed pump power of $P_p = 0\ dBm$ and different signal power levels are shown in Figure 4.1a and Figure 4.1b respectively.

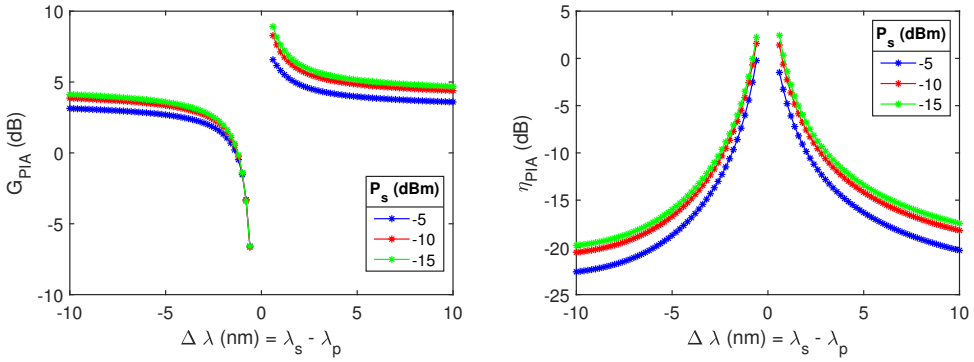

(a) (b)

Figure 4.1: Degenerate pump configuration SOA PIA (a) signal gain spectra for (b) idler conversion efficiency for different signal power levels; $P_p = 0\ dBm$

It can be seen that the gain and the idler conversion efficiency are asymmetric and remain almost the same for different values of signal power. As the signal power ap-

proaches the pump power, a reduction can be noticed in the gain and idler conversion efficiency bandwidth. The dependence of gain and idler conversion efficiency spectra on pump power are plotted in Figure 4.2a and Figure 4.2b respectively for a fixed input signal power of $-20\ dBm$.

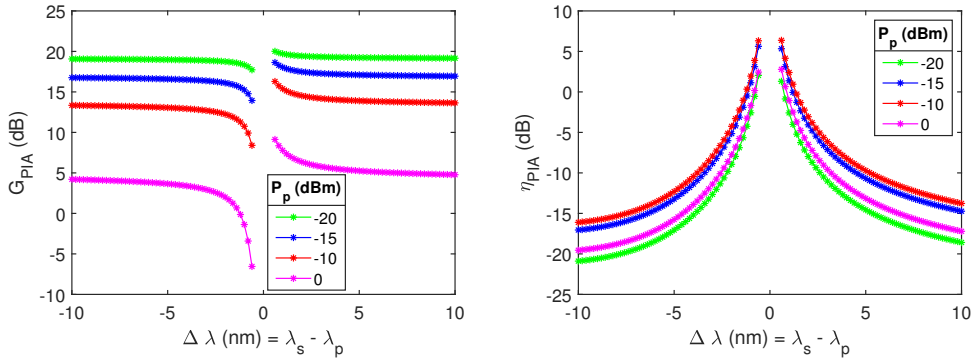

(a) (b)

Figure 4.2: Degenerate pump configuration SOA PIA (a) signal gain spectra (b) idler conversion efficiency for different pump powers; $P_s = -20\ dBm$

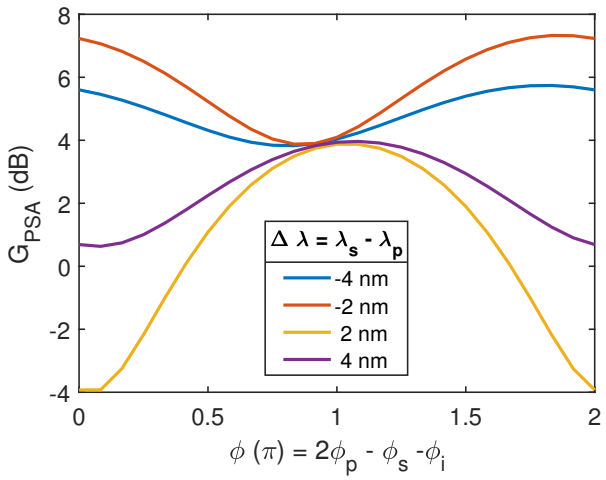

Figure 4.3: PSA signal gain as a function of input phase relation for different wavelength detunings in SOA; $P_p = 0\ dBm$, $P_s = -10\ dBm$

It can be seen that the pump power severely affects the gain spectra as expected. If the pump power and signal power are comparable, there is no significant four wave mixing process happening and hence results in a flat and higher gain for the signal and a lesser idler conversion efficiency. It can be seen that the idler efficiency reduces with the decrease in the pump power as expected. However in the higher regime of the pump power, the idler conversion efficiency decreases because of saturation of SOA. sec:SBSintro In the presence of both signal and idler waves available at the input of SOA, the signal undergoes phase sensitive amplification. The gain experienced by the

signal is plotted as a function of input phase relation ($\phi = 2\phi_p - \phi_s - \phi_i$) in Figure 4.3 for different signal detunings. The idler and signal are assumed to have a same power of $-10\ dBm$ at the input along with a pump power of $0\ dBm$. It can be seen that the signal gain varies as a function of both phase and wavelength similar to that of HNLF (see Section 2.3.2).

4.2 Phase conjugation and signal amplification with modulated data in SOA

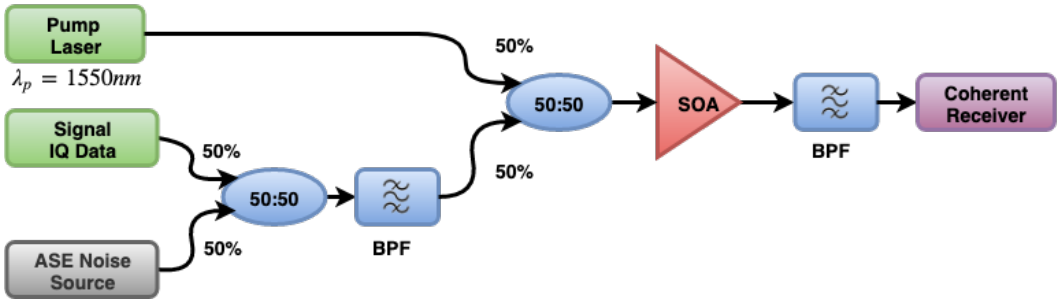

Figure 4.4: Schematic of SOA simulation setup for degenerate pump configuration

In order to deduce the efficacy of SOA as a potential nonlinear medium for communication applications, it is highly important to establish the performance of SOA for phase shift keying signals. The following simulations are executed in MATLAB using Optilux (Serena *et al.* (2009)), the optical simulator toolbox. The schematic of the simulation setup is shown in Figure 4.4 .The pump operating at a wavelength of $1550\ nm$ of linewidth $\Delta f_p = 100kHz$ is assumed. Also, the signal operating a detuning of $f_s - f_p = -150\ GHz$ of linewidth $\Delta f_s = 100\ kHz$ is considered at the input. The signal is modulated with QPSK data of $20\ GBd$ data rate and is assumed to have a simple raised cosine (RC) waveform with zero roll-off factor. The signal is filtered using a Bessel filter of second order with $60\ GHz$ bandwidth in order to eliminate the out-of-band noise. The OSNR of the input signal is modified by adding corresponding noise power to the signal as required. The signal along with the pump is passed through the SOA model as described in the previous section (see Section 4.1.1). To simulate the ASE noise in SOA, a noise variance at quantum levels is also considered at the input of SOA. The received signal and idler are filtered using ideal band pass filters of bandwidth $100\ GHz$ each. A relatively large bandwidth is chosen to capture the

maximum power in the signal or idler. A moving average filer is employed as matched filter to increase the signal to noise ratio (Madhow (2008)) that results in an improved performance. As the input signal and pump lasers are assumed to have phase noise, it is crucial to implement corresponding DSP techniques to recover the phase of the carrier. Hence, a carrier phase recovery technique using fourth power of data (Noe (2005)) is employed in conjunction with Kalman filtering (Kalman (1960)) as the signal contains amplitude noise as well. The parameters considered in the QPSK simulations are also listed in Table.4.2.

Table 4.2: QPSK simulation parameters

Parameter	Value
Signal data-rate	$20\ GBd$
Signal Modulation	NRZ QPSK
NRZ roll-off	0
Number of symbols	2^{16}
Number of samples per symbol	50
Sampling rate	$1000\ GHz\ (1\ ps)$
Pump wavelength	$1550\ nm$
Signal detuning $f_s - f_p$	$-150\ GHz$
Signal laser linewidth	$100\ kHz$
Pump laser linewidth	$100\ kHz$
Input signal filter	Bessel (order 2) of $60\ GHz$ bandwidth
Receiver side signal/ idler filter	Ideal filter of $100\ GHz$ bandwidth

The spectrum of the signal at the input and the output of SOA are plotted in Figure 4.5a and Figure 4.5b respectively. The pump and signal powers considered are $0\ dBm$ and $-10\ dBm$ respectively and the signal has an OSNR of $30\ dB$ at the input. The scatter plot of recieved signal and idler after processing using DSP algorithms are plotted in Figure 4.6a and Figure 4.6b respectively. It can be seen that the signal and idler have a BER of 0 for the given input power and OSNR considerations. Also, it can be noted that the constellation of idler has an angular spread which can be attributed to its broadened line width ($4\Delta f_p + \Delta f_s$) resulting from the phase noise transefer from the pump and the signal. The BER as a function of input signal OSNR is plotted in Figure 4.7 for an input signal power and a pump power of $-10\ dBm$ and $0\ dBm$ respectively. The BER vs OSNR performance is compared against the theoretical BER vs OSNR relationship

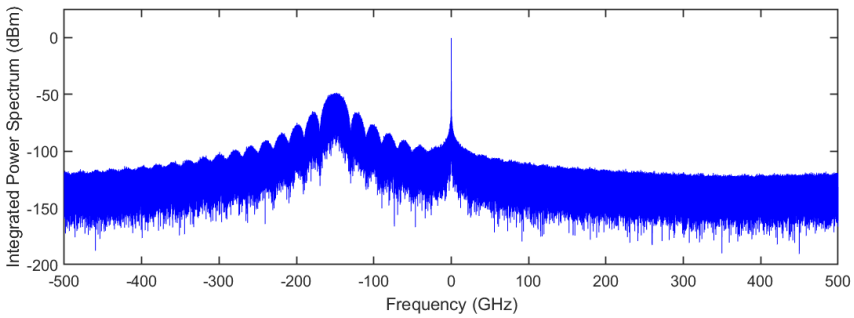

(a)

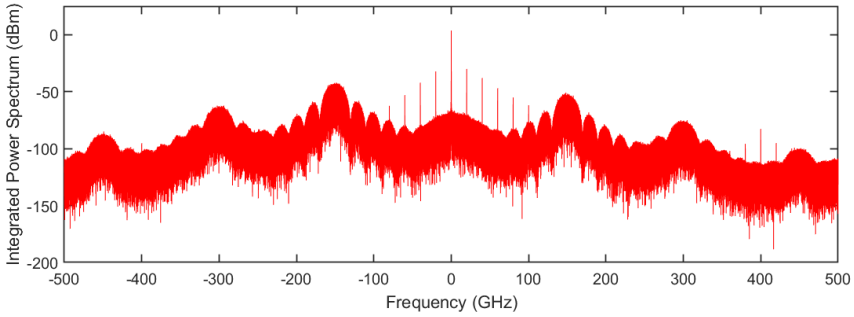

(b)

Figure 4.5: Spectrum at (a) input of SOA (b) output of SOA; $P_p = 0\ dBm$, $P_s = -10\ dBm$, input signal OSNR $= 30\ dB$

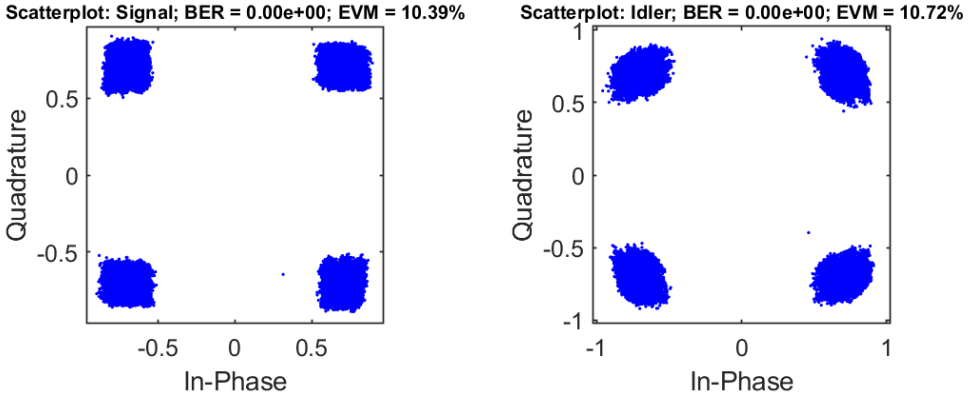

(a) (b)

Figure 4.6: Scatter plot of (a) received signal (b) received idler; $P_p = 0\ dBm$, $P_s = -10\ dBm$, input signal OSNR $= 30\ dB$

for QPSK signal in AWGN channel given by the following expression

$$BER = \frac{1}{2} erfc\left(\sqrt{\frac{E_b}{N_0}}\right)$$
$$OSNR = p\frac{R_s}{2B_{ref}} k\frac{E_b}{N_0} \tag{4.9}$$

where $p = 1$ refers to the number of polarizations involved, $k = 2$ refers to the modulation order, $R_s = 20\ GBd$ refers to the data rate and $B_{ref} = 12.5\ GHz$ refers to the

reference noise bandwidth of $0.1\ nm$ at a center frequency of $1550\ nm$. From Figure 4.7, it can be observed that back-to-back signal performance falls on the theoretical curve as expected. However, the signal and idler at the output of SOA suffers an OSNR penalty compared to the theoretical curve. Also, the OSNR penalty experienced by the idler is larger when compared to that of the signal because of its broadened linewidth.

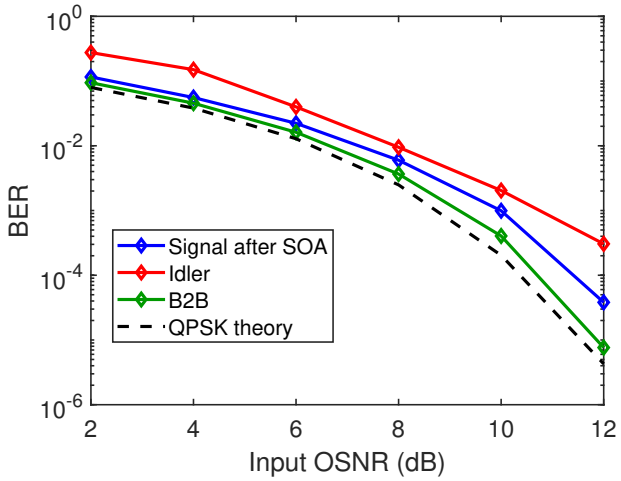

Figure 4.7: BER vs OSNR performance for QPSK data in SOA; $P_p = 0\ dBm$, $P_s = -10\ dBm$

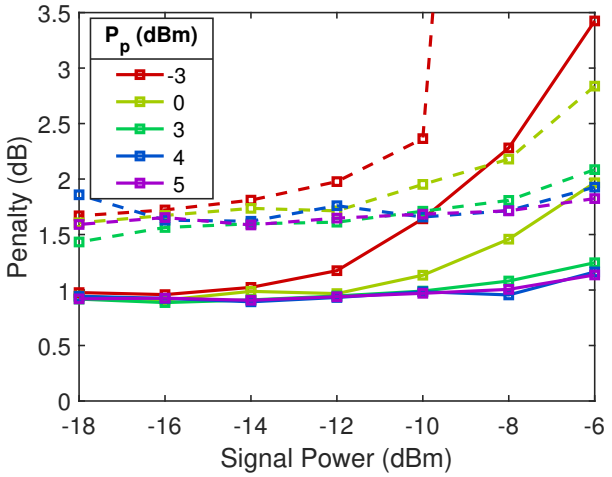

Figure 4.8: OSNR penalty at a BER of 10^{-3} for signal and idler in SOA; solid line represents signal and dashed line represents idler

In order to ascertain the signal and idler performances in SOA for different input conditions, the OSNR penalty experienced by the signal and idler in SOA with respect to theoretical value at a BER of 10^{-3} is plotted in Figure 4.8. It can be seen that the idler experiences a higher penalty for all the power conditions compared to the signal owing to its broadened linewidth. In the higher pump regime, the penalty is lesser for both signal and idler for all signal power levels and remain almost constant because of the

gain saturation in the medium. The gain oscillations is absent in SOA when the pump power dominates over the signal power. However in the lower pump power regime, the OSNR penalty increases drastically when the signal and pump powers are comparable. This can be attributed to the gain oscillations in SOA due to the input signal which is highly prevalent when the signal power is comparable with the pump power. It also has been experimentally shown by Sobhanan *et al.* (2019) that the NF of SOA is $\approx 0\ dB$ for the incoming signal with OSNR in the range of $10\ dB - 30\ dB$. Also, the conjugate also retains the input signal OSNR for values $< 28\ dB$ when $f_s < f_p$. Hence, by choosing appropriate input powers for both signal and pump, it is possible to attain minimal penalty for both signal and idler at the output of SOA, which is desirable for optical signal processing applications.

4.3 Mid-span spectral inversion using optical phase conjugation

Optical phase conjugation (OPC), employed mid-span, is recognized as one of the efficient all-optical methods to mitigate the impairments due to both chromatic dispersion and Kerr nonlinearities in long haul optical fiber links (Minzioni *et al.* (2005), Jansen *et al.* (2006)). Optical phase conjugation employed mid-span creates a spectrally inverted copy of the distorted signal. The pulse evolution in the fiber spans after mid-span OPC, if symmetric to that before of OPC, results in compensation of chromatic dispersion and nonlinear impairments. One of the primary limitations of MSSI is that it is practically difficult to achieve symmetric power profile which makes it impossible to achieve complete compensation of nonlinear impairments. As a consequence of this, the performance of MSSI decreases with the launch power (Minzioni and Schiffini (2005)). Mid-span spectral inversion (MSSI), using phase conjugate generation in HNLF, have been experimentally demonstrated in the past for mitigation of nonlinear impairments in long haul fiber links (Al-Khateeb *et al.* (2018), Solis-Trapala *et al.* (2015)). However, it is exigent to establish the performance of MSSI using SOA for generating the phase conjugate because of its various allied advantages over HNLF which is the primary focus of this section.

4.3.1 MSSI using phase conjugation in SOA

The schematic of MSSI is shown in Figure 4.9. The signal is modulated with QPSK data of parameters listed in Table.4.2 and is launched into the fiber link. Each span is made up of $80\ km$ of fiber subsequently followed by an EDFA of $16\ dB$ gain and $5\ dB$ noise figure. OPC stage is used to obtain the spectrally inverted of the distorted signal at mid-span. The conjugate of the signal is then subsequently passed through the remaining fiber spans before being received using coherent receiver for further processing. The phase conjugation is employed using SOA and the signal is maintained at a detuning of $f_s - f_p = -150\ GHz$ in OPC stage. The pump power and signal power are considered as $3\ dBm$ and $-10\ dBm$ at the input of SOA. The values of power chosen are such that the OSNR penalty experienced by the conjugate (idler) is minimized along with power maximization, based on the discussions held in the previous section (see Section.4.2).

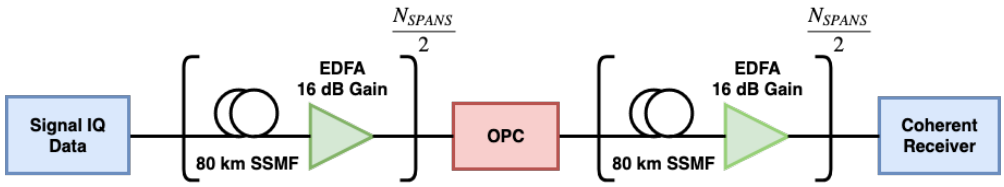

Figure 4.9: Schematic of MSSI

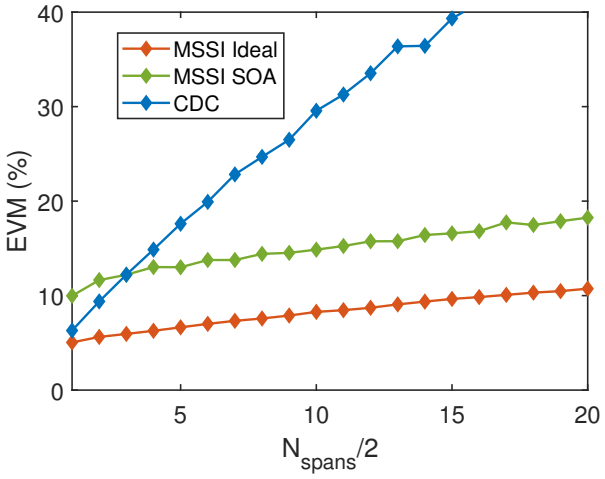

Figure 4.10: MSSI performance as a function of number of spans for a launch power of $3\ dBm$

The best performance that can be achieved using MSSI is by employing an ideal phase conjugator which does not involve any phase noise transfer from the pump and the signal to the generated conjugate. Hence, this sets the theoretically achievable limit for the performance of MSSI. The performance of MSSI using SOA as a function of

number of spans in the link is plotted in Figure 4.10 for a launch power of $3\ dBm$ and is compared against the theoretical limit of MSSI using an ideal phase conjugator. The impairments due to chromatic dispersion can also be electronically compensated using a digital coherent receiver (Savory *et al.* (2007)). Hence, the performance of chromatic dispersion compensation (CDC) technique is also plotted in Figure 4.10 for an insightful comparison. It is clear that CDC does not compensate nonlinear impairments and is expected to perform poorly when compared to MSSI especially in higher power regime. Error vector magnitude (EVM) is used a performance metric as BER is 0 for most of the cases. From Figure 4.10, it can observed that the MSSI using SOA performs poorly when compared to that of MSSI using ideal phase conjugation because of its associated broadened linewidth of the generated conjugate. Also, the performance of MSSI decreases gradually with the number of spans which can be attributed to both ASE noise addition in EDFA and residual uncompensated nonlinear distortions at larger lengths of fiber link. However, the performance of CDC worsens drastically with the number of spans as the nonlinear impairments remains uncompensated.

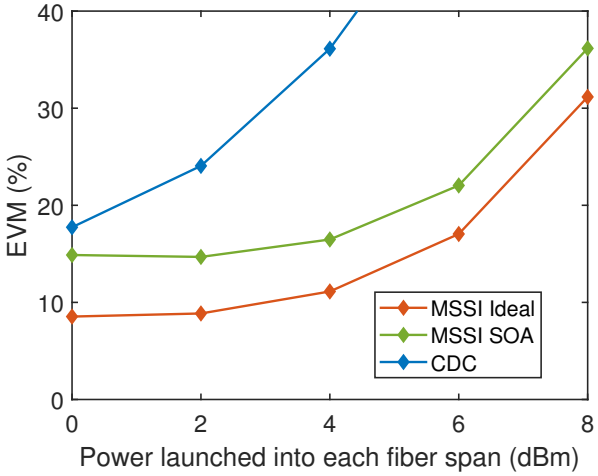

Figure 4.11: MSSI performance as a function of launch power for a fixed number of 10 spans before and after the OPC stage

In order to ascertain the efficacy of MSSI for different launch power levels, the EVM performance of MSSI as a function of launch power is obtained by varying the input launch power for a fixed number of 10 spans before and after the OPC stage and plotted in Figure 4.11. It can be noted that the performance of MSSI worsens significantly with the increase of launch power into the system because of increased uncompensated residual nonlinear impairments, which critically limits the usefulness of MSSI at higher launch power levels ($> 4\ dBm$). However, the performance of CDC

is extremely poorer when compared to MSSI, which illustrates the need for MSSI in long haul optical communication links in order to compensate nonlinear impairments.

Based on the discussions held in this chapter, SOA proves to be one of the potential competitor for optical signal processing applications. The advantages provided by SOA is incontestable besides the fact that ASE noise is present in SOA. However, it has been experimentally demonstrated that the noise addition due to SOA is negligible in the OSNR ranges that are typically involved in the communication links (Sobhanan *et al.* (2019)), which ensures the effectiveness of usage of SOA for nonlinear applications.

CHAPTER 5

Conclusions and Future Work

In this report, a detailed analysis of nonlinear optical amplification in HNLF and SOA have been presented along with the experimental results and simulation results. Based on the discussions and analysis presented in chapter 2, PSA in FOPAs (HNLF) is identified to be one of the prominent ways of realizing low noise amplification in long haul optical communication links. Also, it has been reported in Section 2.2.2 that it requires around $23\ dBm$ of pump power to provide a PIA gain of $\approx 5\ dB$ to the incoming optical signal which requires suppression of SBS in HNLF. The SBS threshold in typical HNLF fiber of $1\ km$ length is around $10\ dBm$, which has been experimentally increased to $\approx 23\ dBm$ by implementing phase modulation of pump laser using three sinusoidal tones. The gain and idler conversion efficiency have been quantified for continuous wave signals in degenerate pump configuration with active SBS suppression. However, phase modulation of pump in degenerate pump configuration results in signification corruption of phase shift keying signals due to the phase noise transfer from the modulation of pump. Hence, a dual pump configuration using counter phase modulation has been experimentally implemented to realize effective amplification and phase conjugation of QPSK signals. The gain and idler conversion efficiency spectra of multiple possible idlers have been experimentally obtained. However, the idler still had phase noise resulting from pump modulation that needs to be analysed further. In order to demonstrate PSA in HNLF, using SOA as a copier stage to generate phase phase locked pump, signal and idler waves can be pursued further. Also, the noise figure of PIA and PSA processes in HNLF should be obtained as a function of input OSNR and should be compared against EDFA to experimentally establish the significance of PA. However, the method of active suppression of SBS in HNLF using phase modulation increases the complexity of the setup. Hence as a future work, dispersion decreasing fibers using dopant variation (Li *et al.* (2005)) can be pursed to increase the SBS threshold passively. However, it will require sophisticated fabrication techniques to realize these special fibers, but provides an irrefutable advantage over active suppression of SBS in HNLF in terms of complexity of the experimental realization.

SOA though non-parametric in nature proves to have an upper hand over fiber based amplifiers in terms of the complexities involved. In chapter 4, the PIA and PSA nature of SOAs have been analysed using simulation results. Also, the simulation results show that SOAs can be actively employed for communication applications involving advanced modulation formats such as QPSK as the penalty provided by SOA for the OSNR ranges typically encountered in the communication links is endurable because of its other associated advantages. Also, the motivation behind MSSI in long haul communication links has been discussed in Section 4.3.1 and MSSI using SOA for optical phase conjugation has been analysed using simulation results. The simulation results shows that SOA can be potentially used in the links as the performance does not deviate significantly from the ideally achievable performance.

APPENDIX A

Experimental Analysis of Noise Transfer in Optical Phase Conjugation Process in Nonlinear SOA

Experimental Analysis of Noise Transfer in Optical Phase Conjugation Process in Nonlinear SOA

Aneesh Sobhanan, Karthik Vijay A.M, Lakshmi Narayanan V, R. David Koilpillai, Deepa Venkitesh*

Department of Electrical Engineering, IIT Madras, India

**deepa@ee.iitm.ac.in*

Abstract: We experimentally evaluate the noise transfer properties during the phase conjugation process in nonlinear SOA by varying the OSNR of the input signal. OSNR retention is observed for both the signal and the conjugate.

OCIS codes: 070.5040, 250.5980, 070.4340

1. Introduction

Optical phase conjugation (OPC) is recognized as one of the efficient methods to mitigate the impairments due to both chromatic dispersion and Kerr nonlinearities in long haul optical fiber transmission systems [1]. Optical phase conjugation is also a critical functionality in achieving phase sensitive amplification (PSA) where a noise figure of smaller than 3 dB is achievable [2]. The second and third order nonlinearities in different nonlinear media such as PPLN, HNLF and dielectric waveguides have been used in the past to successfully demonstrate optical phase conjugation [3–5]. However, the power required to initiate nonlinearities is of the order of tens/hundreds of mW for efficient nonlinear conversion which renders them impractical. Semiconductor optical amplifiers (SOA) on the other hand have proved to be an efficient and compact platform that requires much smaller optical power levels to invoke nonlinearities. In the past, we have demonstrated phase conjugation, wavelength conversion and phase quantization using nonlinear semiconductor optical amplifier (NL-SOA) [6–8].

The gain provided by SOA is fundamentally non-parametric in nature and it is generally perceived that the spontaneous noise introduced by SOA will make it incompetent for applications in nonlinear optical signal processing. In this work, we experimentally evaluate the noise performance of a nonlinear SOA in the context of optical phase conjugation. In most of the previous works, the performance of the generated conjugate was evaluated by noise loading the filtered conjugate and measuring the bit error rate (BER) as a function of the loaded OSNR. These measurements assume a transmitter-class OSNR ($> 25dB$) at the input of the nonlinear medium and does not take into account the noise transfer that could potentially occur due to the phase conjugation process in SOA at various *input* OSNR levels. Since the PSA stage is typically envisaged to be placed mid-span, it is critical to evaluate the noise transfer as a function of the input signal OSNR. PSA also requires a coherent mixing of signal and conjugate at the output of the nonlinear device. In this work, we experimentally study the performance of both the signal and the conjugate at the output of SOA for different *input signal OSNRs* for both continuous wave (CW) and 21 Gbaud QPSK signals.

2. Experimental setup

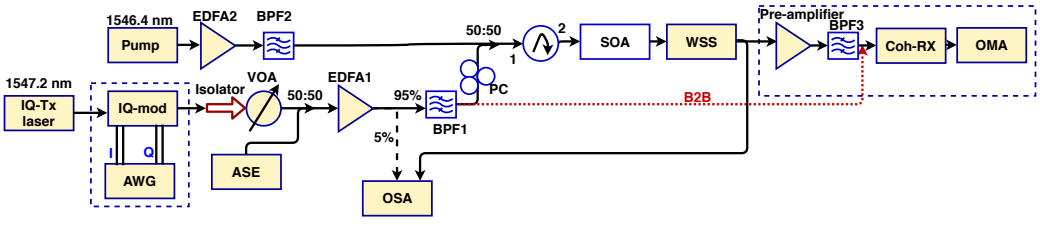

Fig. 1. Experimental setup to study the noise transfer in the phase conjugation process in NL-SOAs (Components inside the dashed box are only included in 21 Gbd QPSK transmission)

The experimental setup for the phase conjugation using nonlinear SOA (Kamelian-NL-SOA, recombination time $\tau_s = 25$ ps) is shown in Fig.1. The pump (frequency: f_p, linewidth: $\Delta f_p = 100$ KHz) is amplified through erbium doped fiber amplifier (EDFA) and is subsequently filtered using a band pass filter (BPF BW: 0.1 nm). The signal (frequency: f_s, linewidth : $\Delta f_s = 40$ KHz) from a tunable laser is noise loaded using an amplified spontaneous emission (ASE) source and is coupled with the pump using a 3 dB coupler and is fed to the nonlinear SOA. In case of experiments with QPSK modulation (21 Gbaud), the signal is fed to an optical IQ modulator driven by an arbitrary waveform generator (65 GSa/s), prior to noise loading. The average power of the pump and the signal are maintained at 0 dBm and -8 dBm

respectively at the input of SOA for both continuous wave (CW) and QPSK modulated signals. The signal frequency is tuned over a frequency offset of $\pm$125 GHz with respect to the pump in order to measure the signal gain and the conjugate conversion efficiency.

For CW case, we observe the output spectra in the OSA (NRT-8000) and measure the OSNR of the signal and the generated conjugate (frequency: $2f_p - f_s$). For the phase modulated signal, the conjugate is observed in the OSA for measuring the OSNR while the output signal and conjugate are filtered independently using waveshaper (WSS-1000s: Finisar) and fed to a phase and polarization diverse coherent receiver. The detected signals (both I and Q) are then digitized using ADC (80 GS/s) and this data is further processed using the standard digital processing algorithms to obtain the BER for different input OSNRs. In all the experiments that involve BER calculations, it is ensured that the power incident on the receiver is maintained constant.

3. Results and discussions

The signal gain and the conjugate conversion efficiency (defined as ratio of output conjugate power to the input signal power) are shown as the function of detuning ($f_s - f_p$) for the CW case in Fig. 2(a). The figure indicates that the conversion efficiency is > 0 dB for a detuning $< \pm 40$ GHz. In addition, the signal is also amplified in the process with a gain of > 10 dB for negative detuning. The signal gain and the conversion efficiency are found to be higher in the negative detuning regime, which is the characteristic of the SOA gain tilt. From Fig. 2(a), it is also possible to identify the exact detuning for which the conjugate and signal powers maintain a specific ratio at the output, which are relevant for PSA applications. We now proceed to experimentally measure the OSNRs of the output signal and the conjugate for a fixed detuing of 100 GHz,, for both positive and negative detuning regimes. This specific detuning was chosen for convenience in filtering and to avoid ambiguity in OSNR measurements. The OSNRs of the output signal and the conjugate are shown in Fig.2(b) for different input signal OSNRs.

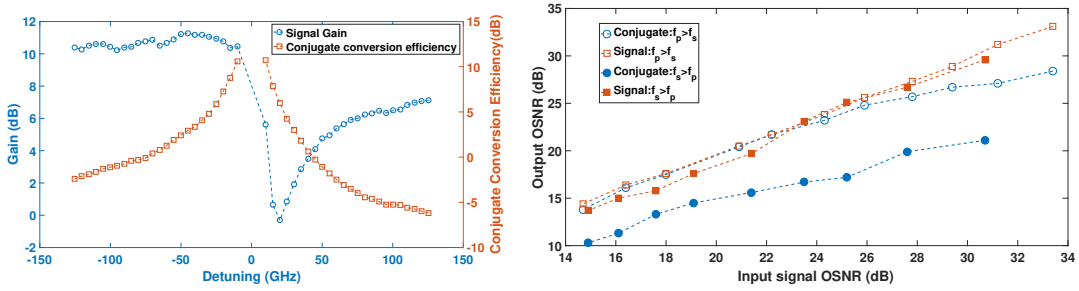

(a) (b)

Fig. 2. (a) Signal gain and conjugate conversion efficiency vs detuning ($f_s - f_p$) for CW signal (b) Output OSNR of the signal and conjugate vs input OSNR for both $f_s < f_p$ and $f_s > f_p$ cases for CW signal

We observe an OSNR retention in the signal after the phase conjugation process in SOA for both $f_s < f_p$ and $f_s > f_p$ cases (Fig.2(b)). For the case $f_s < f_p$, the conjugate retains the input signal OSNR for values < 28 dB, where after it starts to progressively degrade. At larger values of input OSNR the noise floor is dominated by thermal noise, and hence there is a significant ASE noise introduced by the SOA at the conjugate frequency which degrades the OSNR. In case of $f_s > f_p$, the OSNR of the conjugate degrades for the case compared to that of the signal for all values of input OSNR. This can be attributed to its smaller conversion efficiency as evident in Fig. 2(a).

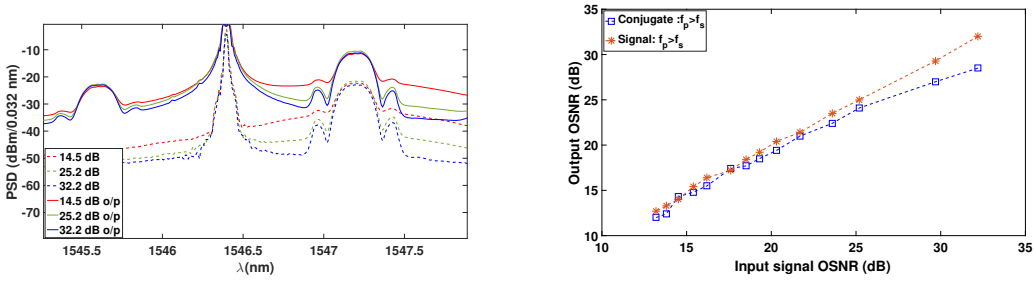

(a) (b)

Fig. 3. (a) SOA input and output spectra for different OSNR values (b) Output OSNR of the signal and the conjugate vs input OSNR for 21 Gbaud QPSK signal ($f_p > f_s$)

We proceed with $f_s < f_p$ configuration for 21 Gbaud QPSK experiment. The input and output spectra at NL-SOA for 21 Gbaud QPSK modulated signal are shown in Fig.3(a). This figure shows that the conjugate of the modulated

signal is generated with a conversion efficiency of around 0 dB and the signal experiences a gain of around 10 dB at a detuning of 100 GHz. The OSNRs of the output signal and the conjugate are shown in Fig.3(b) for different input signal OSNRs. The OSNR performance of the phase modulated data is similar to that of the CW case. For the power levels used in our experiments the effect of noise figure of the NL-SOA is not evident. However, the chirp introduced by the SOA is expected to degrade the quality of the phase modulated data. In order to visualize this, we observe the constellation plots of the amplified signal both in the presence and the absence of pump at two different OSNR values, as shown in Fig.4(a).

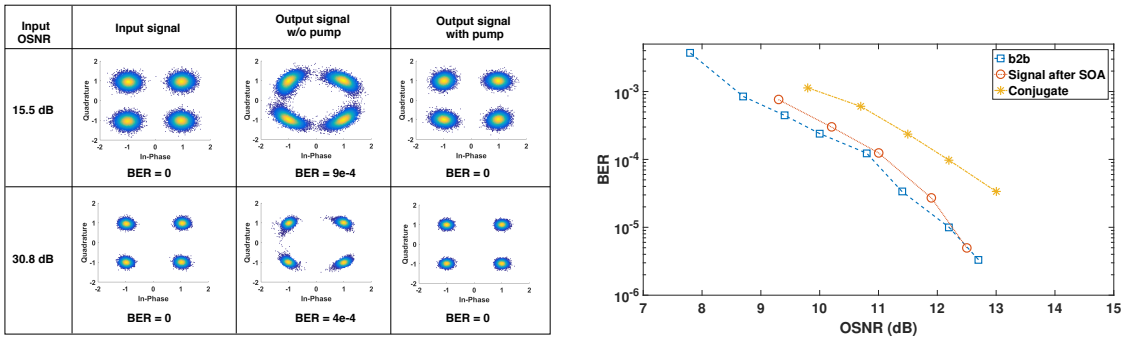

(a) (b)

Fig. 4. (a) Signal constellations at the input, output (without pump), output (with pump) for two OSNR values (15.5 dB and 30.8 dB), (b) BER vs OSNR performance for back-to back, signal after SOA, conjugate

In the absence of pump, signal acquires significant nonlinear phase noise which results in a BER of $\approx$ 1e-4 for both higher and lower OSNR values. However in the presence of pump, it can be seen from the constellation plots that the amplified signal does not undergo any phase distortion, which is corroborated by an improved BER. This implies that the signal does not get affected by the chirp from the nonlinear SOA in the presence of pump.

We now proceed to quantify the influence of chirp in the conjugate by analysing the BER performance as a function of input OSNR, and compare with back to back signal performance for data modulated at 21 Gbaud QPSK. The results are shown in Fig.4(b). The performance of the output signal is identical to that of the back-to-back configuration, thus proving that there is no significant noise addition due to SOA even with a gain of $>$ 10 dB.The generated conjugate is observed to have a penalty of $\approx$1 dB for all OSNR values. This degradation can be attributed to the increased phase noise in the conjugate due to its broadened linewidth ($4\Delta f_p + \Delta f_s$) when compared to the input signal. It should be noted that and this phase noise addition is characteristic of the FWM process with uncorrelated inputs, and not specific to SOA.

4. Conclusion

We demonstrate the amplification of the signal and generation of conjugate without additional noise introduced by the SOA, in phase conjugation process. The variation of output signal and conjugate OSNR is measured for different ONSR levels of the input signal and have proved OSNR retention for both signal and conjugate for detuning conditions where $f_s < f_p$. In the absence of pump, signal amplification in nonlinear SOA is accompanied with nonlinear phase distortions, whereas these distortions are completely suppressed in the presence of the saturating pump. BER evaluated for the output signal and conjugate as a function of input OSNR shows that the signal retains the data quality while the penalty ($<$ 1 dB) observed in the conjugate is only due to the phase noise addition in SOA. The NF of SOA is not of concern under the power levels used for nonlinear applications. Hence, we provide conclusive evidence on the utility of the SOA towards phase conjugation and phase sensitive amplification.

Acknowledgments: This work is supported by The Office of the PSA and the Visvesvaraya PhD Scheme.

References

1. G. Saavedra *et al.*, in "*Optical Fiber Communications Conference and Exposition (OFC)*," (2018), pp. 1–3.
2. M. Karlsson *et al.*, Journal of Lightwave Technology **34**, 1411–1423 (2016).
3. T. Umeki *et al.*, Opt. Express **24**, 16,945–16,951 (2016).
4. M. A. Z. Al-Khateeb *et al.*, Opt. Express **26**, 23,945–23,959 (2018).
5. A. Gajda *et al.*, in "Optical Fiber Communication Conference," (Optical Society of America, 2018), p. W3E.4.
6. A. Sobhanan and D. Venkitesh, Opt. Express **26**, 22,761–22,772 (2018).
7. A. P. Anthur *et al.*, Opt. Express **24**, 11,749–11,761 (2016).
8. K. R. H. Bottrill *et al.*, IEEE Photonics Technology Letters **28**, 205–208 (2016).

APPENDIX B

MATLAB codes for the simulations

B.1 SOA Model

```
%Author Sean O Duill
function [ hdot ] = dhdt( soa, p_in, h_in )
% calculates the SOA rate equation for the time
% derivative for the SOA gain coefficient

hdot = (soa.h0 - h_in)/soa.tau_s - (h_in/(h_in-soa.loss))*...
    p_in*(exp(h_in-soa.loss)-1)/(soa.p_sat*soa.tau_s);
end
% ------------------------------------------------------------------
%Author Sean O Duill
function [ h_new ] = solve_h( soa, timestep, p_in, h_in)
%Predictor-Corrector method to solve for h
%   calculate one euler step, use this value to perform another euler step.
%   then the updated value for h depends on the average of these two values

dh1 = dhdt(soa, p_in, h_in);
h_dash = dh1*timestep + h_in;
dh2 = dhdt(soa, p_in, h_dash);
h_new = 0.5*(dh1+dh2)*timestep + h_in;
end
% ------------------------------------------------------------------
function [ soa_out_field] = soa_block( soa,timestep, e_in )
% This function reads in a electric field signal and calculates the
% output electric field signal at the output of an SOA. input electric
% field assumed to be complex in nature due to advanced md. formats.
% timestep = 1e-12; % determines the signal sampling rate and the timestep
% to solve SOA rate equation
% soa = soa_spec ;%soa = struct( 'loss', 2, 'h0', 8, 'alpha', 4, ...
% 'tau_s', 'p_sat', 0.01); % soa paramters loss, unsaturated gain coeff,
% alpha factor, , carrier lifetime, and saturation power
```

```
N = length(e_in);
p_in = abs(e_in).^2;% calculate the power (intensity) of the incoming wave;
h_t = zeros(1,N); %create array for h(t)
h_in = soa.h0; % Initialise h to be the unsaturated gain coefficient

for a = 1:N %calculates the SOA gain as a function of time
    h_t(a) = solve_h(soa, timestep, p_in(a), h_in);
    h_in = h_t(a); % updates h
end

del_h_ch =-1*h_t./(h_t-soa.loss).*(exp(h_t-soa.loss)-1).*p_in*soa.eps_ch;
del_h_shb =-1*h_t./(h_t-soa.loss).*(exp(h_t-soa.loss)-1).*p_in*soa.eps_shb;

% multiply the input field by the complex valued SOA gain
% (including alpha) to get the output field
soa_out_field = e_in.*exp(0.5*(-1*soa.loss + h_t.*(1-1i*soa.alpha)+...
    del_h_ch.*(1-1i*soa.alpha_ch)+del_h_shb.*soa.eps_shb));

end
```

B.2 QPSK simulations in SOA

```
%Author Karthik Vijay Annur Myilswamy and Anirudh Vijay
function [Sig,Sig_Rx,Idler_Rx,B2B] = SOA_QPSK(Sig,OSNR_dB,Pump,soa)
%% Constants
addpath('..\..\optilux_v0.1\Optilux_files\')
c = 3e8;

%% Pump parameters
lam_p = Pump.lam_p; %in nm
P_pump = Pump.pow; %in watt
f_p = c/lam_p;
lw_pump = 100e3/1e9;

%% Signal parameters
Sig.P_sig_dbm = -8;
Sig.P_sig = 1e-3*10^(Sig.P_sig_dbm/10); % in watt
Sig.OSNR_dB = 20;
Sig.Symbrate = 20;  % Symbol rate
Sig.ModOrder = 2;
```

```
%% System
Sig.Nsymb = 2^14;   % Number of symbols
spect.T = Sig.Nsymb/(Sig.Symbrate/1000); %in picoseconds
spect.dt = 1; %in picoseconds
spect.t = -spect.T/2 + (0:spect.dt:spect.T-spect.dt);...
    % Time axis from -T/2 to T/2 with sampling dt
spect.fs = 1000/spect.dt; % Sampling frequency in GHz
spect.df = 1000/spect.T; % in GHz
spect.f = (-spect.fs/2 + (0:spect.df:spect.fs-spect.df));
% fprintf('\nTime window = %2.1f ps\n',spect.T)
% fprintf('Sampling frequency = %u GHz\n',spect.fs)
spect.Npts = length(spect.t);
Sig.Nt = 1000/(spect.dt*Sig.Symbrate);
Sig.lw = 100e3/1e9;

%% Detuning
Delf_sig = Sig.Delf; % in GHz
[val,ind] = min(abs(Delf_sig - spect.f));
Delf_sig = spect.f(ind);
f_s = f_p - Delf_sig;
f_i = 2*f_p - f_s;
Sig.lam_s = c/f_s;

%% Optilux Setup
reset_all(Sig.Nsymb, Sig.Nt, 1);
duty     = 1;    % duty cycle
roll     = 0;  % pulse roll-off

%% Generating data
Sig.Symbs = qammod(randi([0,2^Sig.ModOrder-1],1,Sig.Nsymb),2^Sig.ModOrder);
Sig.bits  = qamdemod(Sig.Symbs,2^Sig.ModOrder,'OutputType','bit');
E_i = electricsource(Sig.bits(1,:),'bpsk',Sig.Symbrate,'cosroll',duty,roll)
E_q = electricsource(Sig.bits(2,:),'bpsk',Sig.Symbrate,'cosroll',duty,roll)
E_i = circshift(E_i,ceil(Sig.Nt/2));
E_q = circshift(E_q,ceil(Sig.Nt/2)); % Generation of I and Q symbols

del_phi_laser_sig = randn(length(E_i),1)*sqrt(2*pi*Sig.lw*spect.dt/1000);
phi_laser_sig = cumsum(del_phi_laser_sig);
E_sig_laser = ones(length(E_i),1).*exp(1j*phi_laser_sig);...
```

```
    %Adding phase noise

sig_sig = qi_modulator(E_sig_laser,E_i,-E_q).';
sig_sig = sig_sig/rms(sig_sig)*sqrt(1e-3*db2pow(Sig.P_sig_dbm));

%% Noise Loading in Signal
NP = Sig.P_sig_dbm - OSNR_dB; % Noise in 0.1nm in dBm
NP_tot = 10*log10(spect.fs/12.5) + NP; % Total Noise Power in dBm
Noise_add = ((randn(size(sig_sig)) + ...
    1j*randn(size(sig_sig)))*sqrt(0.5*1e-03*db2pow(NP_tot))/sqrt(2));
b2b_sig = sig_sig + Noise_add;
b2b_sig_freq = fftshift(fft(b2b_sig));

%% Signal Filtering
[b,a] = besself(2,30);
fil_freq = abs(freqs(b,a,spect.f));
sig_fil_freq1 = fil_freq.*b2b_sig_freq;
sig_sig_filt = ifft(ifftshift(sig_fil_freq1));

%% Generating Pump
del_phi_laser_pump = randn(length(E_i),1)*sqrt(2*pi*lw_pump*spect.dt/1000);
phi_laser_pump = cumsum(del_phi_laser_pump).';
pump_sig = ones(1,spect.Npts).*exp(1j*phi_laser_pump)*sqrt(P_pump);
pump_sig_freq = fftshift(fft(pump_sig))/length(pump_sig);

%% Generating total signal
total_sig = pump_sig + sig_sig_filt.*exp(1j*2*pi*Delf_sig*spect.t/1000);

%% SOA
total_sig_prop = conj(soa_block(soa,spect.dt*1e-12,conj(total_sig)));
total_sig_prop_freq = fftshift(fft(total_sig_prop));

%% Filtering of B2B Signal
BW_fil = 100;
Fil_sig_b2b = ones(1,length(spect.f));
Fil_sig_b2b(abs(spect.f)>BW_fil/2) = 0;
b2bsig_fil_freq = b2b_sig_freq.*Fil_sig_b2b;
b2bsig_fil = ifft(ifftshift(b2bsig_fil_freq));
b2bsig_fil1 = movsum(b2bsig_fil,Sig.Nt);
```

```
%% Filtering of Signal
Fil_sig = ones(1,length(spect.f));
Fil_sig(abs(spect.f-Delf_sig)>BW_fil/2) = 0;
sig_fil_freq = total_sig_prop_freq.*Fil_sig;
sig_fil_freq = circshift(sig_fil_freq,-Delf_sig/spect.df).*conj(fil_freq);
sig_fil = ifft(ifftshift(sig_fil_freq));
sig_fil1 = movsum(sig_fil,Sig.Nt);
start_pt = ceil(Sig.Nt/2);

sig1 = sig_fil1((Sig.Nt+start_pt):Sig.Nt:(101*Sig.Nt+start_pt));
sig1_tx = sig_sig((Sig.Nt+start_pt):Sig.Nt:(101*Sig.Nt+start_pt));
rotn = sig1./sig1_tx;
sig_fil1 = sig_fil1*exp(-1j*angle(mean(rotn)));
eyediagram(sig_fil1(start_pt+1:start_pt+1000),Sig.Nt); % Eye diagram
title('Eye Diagram: Signal, Post SOA')

%% Filtering of Idler
Fil_idler = ones(1,length(spect.f));
Fil_idler(abs(spect.f+Delf_sig)>BW_fil/2) = 0;
sig_idler_freq = total_sig_prop_freq.*Fil_idler;
sig_idler_freq = circshift(sig_idler_freq,+Delf_sig/spect.df).*fil_freq;
idler_fil = ifft(ifftshift(sig_idler_freq));
idler_fil1 = movsum(idler_fil,Sig.Nt);
start_pt = ceil(Sig.Nt/2);

idler1 = idler_fil1((Sig.Nt+start_pt):Sig.Nt:(101*Sig.Nt+start_pt));
sig1_tx = sig_sig((Sig.Nt+start_pt):Sig.Nt:(101*Sig.Nt+start_pt));
rotn = idler1./conj(sig1_tx);
idler_fil1 = idler_fil1*exp(-1j*angle(mean(rotn)));
eyediagram(idler_fil1(1+start_pt:1000+start_pt),Sig.Nt);
title('Eye Diagram: Idler, Post SOA')

%% Demodulation of B2B signal
b2bsig_rx_symbs = b2bsig_fil1(start_pt:Sig.Nt:end);
b2bsig_rx_symbs = b2bsig_rx_symbs/rms(b2bsig_rx_symbs);

theta = 0;   % Kalman Filering and carrier phase recovery
P = 0;
Q = 2*pi*(4*lw_pump+Sig.lw)*spect.dt/1000;
A = 1;
```

```
H = 1;
R = 1/db2pow(OSNR_dB);
for ii = 1:length(b2bsig_rx_symbs)
    theta4 = angle((b2bsig_rx_symbs(ii)*exp(-1j*theta)).^4);
    if theta4>0
        th = (theta4 - pi)/4;
    else
        th = (theta4 + pi)/4;
    end
    theta0 = theta + th;
    apriori_ErrorCovariance = A*P*A' + Q;
    K = apriori_ErrorCovariance*H'/(H*apriori_ErrorCovariance*H' + R);
    theta = theta + K*(theta0 - theta);
    P = apriori_ErrorCovariance - K*H*apriori_ErrorCovariance;

    b2bsig_rx_symbs(ii) = b2bsig_rx_symbs(ii)*exp(-1j*theta);
end

b2bsig_bits_rx = qamdemod(b2bsig_rx_symbs,2^Sig.ModOrder,...
    'UnitAveragePower',true,'OutputType','bit');
ber_b2b = sum(sum(b2bsig_bits_rx~=Sig.bits))/numel(Sig.bits);
evm_b2b = rms(b2bsig_rx_symbs - Sig.Symbs/sqrt(2));

%% Demodulation of signal after SOA
sig_rx_symbs = sig_fil1(start_pt:Sig.Nt:end);
sig_rx_symbs = sig_rx_symbs/rms(sig_rx_symbs);

theta = 0;  % Kalman Filering and carrier phase recovery
P = 0;
Q = 2*pi*(4*lw_pump+Sig.lw)*spect.dt/1000;
A = 1;
H = 1;
theta_set = zeros(size(sig_rx_symbs));
for ii = 1:length(sig_rx_symbs)
    theta4 = angle((sig_rx_symbs(ii)*exp(-1j*theta)).^4);
    if theta4>0
        th = (theta4 - pi)/4;
    else
        th = (theta4 + pi)/4;
    end
```

```
    theta0 = theta + th;
    apriori_ErrorCovariance = A*P*A' + Q;
    K = apriori_ErrorCovariance*H'/(H*apriori_ErrorCovariance*H' + R);
    theta = theta + K*(theta0 - theta);
    P = apriori_ErrorCovariance - K*H*apriori_ErrorCovariance;
    theta_set(ii) = theta;
    sig_rx_symbs(ii) = sig_rx_symbs(ii)*exp(-1j*theta);
end

sig_bits_rx = qamdemod(sig_rx_symbs,2^Sig.ModOrder,...
    'UnitAveragePower',true,'OutputType','bit');
ber_sig = sum(sum(sig_bits_rx~=Sig.bits))/numel(Sig.bits);
evm_sig = rms(sig_rx_symbs - Sig.Symbs/sqrt(2));

%% Demodulation of idler
idler_rx_symbs = conj(idler_fill(start_pt:Sig.Nt:end));
idler_rx_symbs = idler_rx_symbs/rms(idler_rx_symbs);
% idler_rx_symbs = adapt_LN(idler_rx_symbs,4);

theta = 0;   % Kalman Filering and carrier phase recovery
P = 0;
Q = 2*pi*(4*lw_pump+Sig.lw)*spect.dt/1000;
A = 1;
H = 1;
theta_set = zeros(size(idler_rx_symbs));
for ii = 1:length(idler_rx_symbs)
    theta4 = angle((idler_rx_symbs(ii)*exp(-1j*theta)).^4);
    if theta4>0
        th = (theta4 - pi)/4;
    else
        th = (theta4 + pi)/4;
    end
    theta0 = theta + th;
    apriori_ErrorCovariance = A*P*A' + Q;
    K = apriori_ErrorCovariance*H'/(H*apriori_ErrorCovariance*H' + R);
    theta = theta + K*(theta0 - theta);
    P = apriori_ErrorCovariance - K*H*apriori_ErrorCovariance;
    theta_set(ii) = theta;
    idler_rx_symbs(ii) = idler_rx_symbs(ii)*exp(-1j*theta);
end
```

```
idler_bits_rx = qamdemod(idler_rx_symbs,2^Sig.ModOrder,...
    'UnitAveragePower',true,'OutputType','bit');
ber_idler = sum(sum(idler_bits_rx~=Sig.bits))/numel(Sig.bits);
evm_idler = rms(idler_rx_symbs - Sig.Symbs/sqrt(2));

Sig_Rx.Symbs = sig_rx_symbs;
Sig_Rx.ber = ber_sig;
Sig_Rx.evm = evm_sig;
Idler_Rx.Symbs = idler_rx_symbs;
Idler_Rx.ber = ber_idler;
Idler_Rx.evm = evm_idler;
B2B.ber = ber_b2b;
B2B.evm = evm_b2b;
B2B.Symbs = b2bsig_rx_symbs;

%% Scatter plots of signal after SOA and idler
scatterplot(sig_rx_symbs);
title(['Scatterplot: Signal; BER = ' num2str(ber_sig,'%.2e')...
    '; EVM = ' num2str(evm_sig*100,'%.2f') '%']);
scatterplot(idler_rx_symbs);
title(['Scatterplot: Idler; BER = ' num2str(ber_idler,'%.2e')...
    '; EVM = ' num2str(evm_idler*100,'%.2f') '%']);

end
```

B.3 MSSI in SOA with QPSK data simulations

```
%Author Karthik Vijay Annur Myilswamy and Anirudh Vijay
function Idler_Rx = MSSI_spans_SOA(span_length,Nspan)

c = 299792458;                          % speed of light (m/s)
lambda_0 = 1550;                        % center wavelength (nm)
f_0 = c/lambda_0;

% global CONSTANTS;             % CONSTANTS is a global structure variable.
CLIGHT  = c;  % Speed of light in vacuum [m/s]
HPLANCK = 6.626068960000000e-34; % Planck's constant [J*s]
%% SOA parameters
G = 10;
g = 10^(G/10);
```

```
soa = struct('loss', 4, 'h0', g, 'alpha', 4, 'tau_s', 25e-12, 'p_sat', 0.002);
soa.eps_ch = 0.5;
soa.alpha_ch = 2;
soa.eps_shb = 2;

%% Pump parameters
lam_p = 1550e-9; %in nm, center frequency
f_p = c/lam_p;
P_pump = 2;   %in mW
%% Signal parameters

Sig.P_sig_dbm = 3;
Sig.P_sig = 1e-3*10^(Sig.P_sig_dbm/10); % in watt

% Sig.OSNR_dB = 1000;
Sig.Symbrate = 20;                    % Symbol rate
Sig.ModOrder = 2;
%% System Paarameters
Sig.Nsymb = 2^14;   % Number of symbols
spect.T = Sig.Nsymb/(Sig.Symbrate/1000); %in picoseconds
spect.dt = 1; %in picoseconds
spect.t = -spect.T/2 + (0:spect.dt:spect.T-spect.dt);...
    % Time axis from -T/2 to T/2 with sampling dt
spect.fs = 1000/spect.dt; % Sampling frequency in GHz
spect.df = 1000/spect.T; % in GHz
spect.f = (-spect.fs/2 + (0:spect.df:spect.fs-spect.df));
fprintf('\nTime window = %2.1f ps\n',spect.T)
fprintf('Sampling frequency = %u GHz\n',spect.fs)
spect.Npts = length(spect.t);
Sig.Nt = 1000/(spect.dt*Sig.Symbrate);


%% Detuning
Delf_sig = -150; % in GHz
[val,ind] = min(abs(Delf_sig - spect.f));
Delf_sig = spect.f(ind);
f_s = f_p - Delf_sig*1e9;
f_i = 2*f_p - f_s;

Sig.lam_s = c/f_s;
```

```
%% Optilux Setup
duty      = 1;                % duty cycle
roll      = 0;                % pulse roll-off
Psig      = Sig.P_sig*1000;   % Transmitted power per channel [mW]
lam       = Sig.lam_s*1e9;        % Central wavelength [nm]
spac      = Delf_sig/125;     % Channel spacing [nm]
symbrate  = Sig.Symbrate;     % Symbol rate [Gbaud]
Nt        = Sig.Nt;           % Points x symbol
reset_all(Sig.Nsymb, Nt, 1);
laser.single = true;
laser.linewidth = 100e3;
global GSTATE;
%%  Fiber (Tx)
fiber_ph.length  = span_length;          % length [m]
fiber_ph.alphadB = 0.2;              % attenuation [dB/km]
fiber_ph.aeff    = 80;       % effective area [um^2]
fiber_ph.n2      = 2.7e-20; % nonlinear index
fiber_ph.lambda  = 1550;     % wavelength [nm] @ dispersion
fiber_ph.disp    = 17;       % dispersion [ps/nm/km] @ wavelength
fiber_ph.slope   = 0;        % slope [ps/nm^2/km] @ wavelength
fiber_ph.dphimax = 5E-3;     % maximum nonlinear phase rotation per step
fiber_ph.dzmax   = 2E4;      % maximum SSFM step

%% Modulator Parameters
modulator.bias = [0 0];              % Modulator bias point
modulator.amplitude = [1 1];         % Amplitude normalized to V_pi voltage
modulator.exratio = [30 30];       % Modulator extinction

%% Generating data
Sig.Symbs = qammod(randi([0,2^Sig.ModOrder-1],1,Sig.Nsymb),2^Sig.ModOrder);
Sig.bits  = qamdemod(Sig.Symbs,2^Sig.ModOrder,'OutputType','bit');
E_i = electricsource(Sig.bits(1,:),'bpsk',Sig.Symbrate,'cosroll',duty,roll);
E_q = electricsource(Sig.bits(2,:),'bpsk',Sig.Symbrate,'cosroll',duty,roll);
E_i = circshift(E_i,ceil(Sig.Nt/2));
E_q = circshift(E_q,ceil(Sig.Nt/2));
del_phi = randn(size(E_i))*sqrt(2*pi*laser.linewidth*spect.dt*1e-12);
phi_pn = cumsum(del_phi);  % Phase noise

E_sig_laser = lasersource(Psig, lam, spac).*exp(1j*phi_pn); % Laser source
sig_sig = qi_modulator(E_sig_laser,E_i,-E_q,modulator);
```

```
create_field('unique',sig_sig,[],struct('power','average'));

%% Fiber Propagation
GSTATE.SYMBOLRATE = symbrate;
ampli.f = 5;
G_amp   = fiber_ph.alphadB*fiber_ph.length/1e3; % ampli gain [dB]
init_OSNR = 30;
Gerbio = 1;          % Dummy gain
nampli = 1;          % Number of amplifiers
osnrbw = 0.1;        % Bandwidth for OSNR measurement [nm]

hvdl = -30-10*log10(HPLANCK*CLIGHT/lam*CLIGHT*osnrbw/lam^2*1e18);
nsp  = 10*log10(Psig)+hvdl-10*log10(10^(Gerbio/10)-1)-3-10*log10(nampli)-init_OSNR
ampli_OSNR.f = nsp + 3;
ampliflat(-Gerbio,'gain');
ampliflat(+Gerbio,'gain',ampli_OSNR);  % Setting initial OSNR

for ii = 1:Nspan
        fiber(fiber_ph,'g-s-');
        ampliflat(G_amp,'gain',ampli);

end

%% MSSI
FFX = fftshift(fft(GSTATE.FIELDX));
% FFY = fftshift(fft(GSTATE.FIELDY));
[b,a] = besself(2,100);
fil_freq = abs(freqs(b,a,spect.f)).';
FFX = fil_freq.*FFX;
%FFY = fil_freq.*FFY;
GSTATE.FIELDX = ifft(ifftshift(FFX));

sig_to_soa = ifft(ifftshift(circshift(FFX,+Delf_sig/spect.df)));

pump_sig = ones(1,spect.Npts)*sqrt(P_pump);
pump_sig_freq = fftshift(fft(pump_sig))/length(pump_sig);

% Generating total signal
P_sig_req = 10^(-10/10);  % in mW
total_sig = (pump_sig.' + sig_to_soa*(sqrt(P_sig_req)/rms(sig_to_soa)))*sqrt(1e-3
```

```
f = figure();
total_sig_freq1 = fftshift(fft(total_sig))/length(total_sig);
plot(spect.f,20*log10(abs(total_sig_freq1))+30,'b','DisplayName','I/P');
xlabel('Frequency (GHz)');
ylabel('Integrated Power Spectrum (dBm)');


% SOA
total_sig_prop = (conj(soa_block_noise(soa,spect.dt*1e-12,conj(total_sig.')))).'*sqrt(10
total_sig_prop_freq = fftshift(fft(total_sig_prop));
BW_fil = 100;
fil_freq_idler = ones(length(spect.f),1);
fil_freq_idler(abs(spect.f+Delf_sig)>BW_fil/2) = 0;
conj_idler = fil_freq_idler.*total_sig_prop_freq;
conj_idler_shift = circshift(conj_idler,Delf_sig/spect.df);
%FFY = fil_freq.*FFY;
conj_idler_shift = ifft(ifftshift(conj_idler_shift));
GSTATE.FIELDX = conj_idler_shift*sqrt(Sig.P_sig*1000)/rms(conj_idler_shift);

%%
for ii = 1:Nspan
        fiber(fiber_ph,'g-s-');
        ampliflat(G_amp,'gain',ampli);
end

total_sig_prop = GSTATE.FIELDX.';
total_sig_prop_freq = fftshift(fft(total_sig_prop));

%% Filtering of B2B Signal
b2b_sig_freq = fftshift(fft(sig_sig)).';
BW_fil = 100;
Fil_sig_b2b = ones(1,length(spect.f));
Fil_sig_b2b(abs(spect.f)>BW_fil/2) = 0;
b2bsig_fil_freq = b2b_sig_freq.*Fil_sig_b2b;

b2bsig_fil = ifft(ifftshift(b2bsig_fil_freq));
b2bsig_fil1 = movsum(b2bsig_fil,Sig.Nt);
```

```
%% Filtering of Idler

Fil_idler = ones(1,length(spect.f));
Fil_idler(abs(spect.f)>BW_fil/2) = 0;
sig_idler_freq = total_sig_prop_freq.*Fil_idler;

idler_fil = ifft(ifftshift(sig_idler_freq));
idler_fil1 = movsum(idler_fil,Sig.Nt);
start_pt = ceil(Sig.Nt/2);

idler1 = idler_fil1((Sig.Nt+start_pt):Sig.Nt:(101*Sig.Nt+start_pt));
sig1_tx = sig_sig((Sig.Nt+start_pt):Sig.Nt:(101*Sig.Nt+start_pt)).';
rotn = idler1./conj(sig1_tx);
idler_fil1 = idler_fil1*exp(-1j*angle(mean(rotn)));


%% Demodulation of B2B signal
h = 6.626068960000000e-34;
nu = 3e8/1550e-9;
del_nu = 12.5e9;
OSNR_dB = pow2db(Sig.P_sig/(Nspan*db2pow(5)*h*nu*del_nu*10^1.6));

b2bsig_rx_symbs = b2bsig_fil1(start_pt:Sig.Nt:end);
b2bsig_rx_symbs = b2bsig_rx_symbs/rms(b2bsig_rx_symbs);

theta = 0;  % Kalman filtering and carrier phase recovery
P = 0;
Q = 2*pi*(laser.linewidth)*spect.dt*1e-12;
A = 1;
H = 1;
R = 1/db2pow(OSNR_dB);
for ii = 1:length(b2bsig_rx_symbs)
    theta4 = angle((b2bsig_rx_symbs(ii)*exp(-1j*theta)).^4);
    if theta4>0
        th = (theta4 - pi)/4;
    else
        th = (theta4 + pi)/4;
    end
    theta0 = theta + th;
    apriori_ErrorCovariance = A*P*A' + Q;
```

```
    K = apriori_ErrorCovariance*H'/(H*apriori_ErrorCovariance*H' + R);
    theta = theta + K*(theta0 - theta);
    P = apriori_ErrorCovariance - K*H*apriori_ErrorCovariance;

    b2bsig_rx_symbs(ii) = b2bsig_rx_symbs(ii)*exp(-1j*theta);
end

b2bsig_bits_rx = qamdemod(b2bsig_rx_symbs,2^Sig.ModOrder,...
    'UnitAveragePower',true,'OutputType','bit');
ber_b2b = sum(sum(b2bsig_bits_rx~=Sig.bits))/numel(Sig.bits);
evm_b2b = rms(b2bsig_rx_symbs - Sig.Symbs/sqrt(2));

%% Demodulation of propagated signal
idler_rx_symbs = conj(idler_fil1(start_pt:Sig.Nt:end));
idler_rx_symbs = idler_rx_symbs/rms(idler_rx_symbs);

theta = 0;  % Kalman filtering and carrier phase recovery
P = 0;
Q = 2*pi*(laser.linewidth)*spect.dt*1e-12;
A = 1;
H = 1;
theta_set = zeros(size(idler_rx_symbs));
for ii = 1:length(idler_rx_symbs)
    theta4 = angle((idler_rx_symbs(ii)*exp(-1j*theta)).^4);
    if theta4>0
        th = (theta4 - pi)/4;
    else
        th = (theta4 + pi)/4;
    end
    theta0 = theta + th;
    apriori_ErrorCovariance = A*P*A' + Q;
    K = apriori_ErrorCovariance*H'/(H*apriori_ErrorCovariance*H' + R);
    theta = theta + K*(theta0 - theta);
    P = apriori_ErrorCovariance - K*H*apriori_ErrorCovariance;
    theta_set(ii) = theta;
    idler_rx_symbs(ii) = idler_rx_symbs(ii)*exp(-1j*theta);
end

idler_bits_rx = qamdemod((idler_rx_symbs),2^Sig.ModOrder,...
    'UnitAveragePower',true,'OutputType','bit');
```

```
ber_idler = sum(sum(idler_bits_rx~=Sig.bits))/numel(Sig.bits);
evm_idler = rms(idler_rx_symbs - Sig.Symbs/sqrt(2));

Idler_Rx.Symbs = idler_rx_symbs;
Idler_Rx.ber = ber_idler;
Idler_Rx.evm = evm_idler;
B2B.ber = ber_b2b;
B2B.evm = evm_b2b;
B2B.Symbs = b2bsig_rx_symbs;
end
```

REFERENCES

1. **Abedin, K.**, **T. Taunay**, **M. Fishteyn**, **M. Yan**, **B. Zhu**, **J. Fini**, **E. Monberg**, **F. Dimarcello**, and **P. Wisk** (2011). Amplification and noise properties of an erbium-doped multicore fiber amplifier. *Optics express*, **19**(17), 16715–16721.

2. **Agrawal, G. P.** (1988). Population pulsations and nondegenerate four-wave mixing in semiconductor lasers and amplifiers. *JOSA B*, **5**(1), 147–159.

3. **Agrawal, G. P.**, Nonlinear fiber optics. *In Nonlinear Science at the Dawn of the 21st Century*. Springer, 2000, 195–211.

4. **Agrawal, G. P.** and **N. A. Olsson** (1989). Self-phase modulation and spectral broadening of optical pulses in semiconductor laser amplifiers. *IEEE Journal of Quantum Electronics*, **25**(11), 2297–2306.

5. **Al-Khateeb, M. A.**, **M. Tan**, **M. A. Iqbal**, **A. Ali**, **M. E. McCarthy**, **P. Harper**, and **A. D. Ellis** (2018). Experimental demonstration of 72% reach enhancement of 3.6 tbps optical transmission system using mid-link optical phase conjugation. *Optics express*, **26**(18), 23960–23968.

6. **Anderson, B.**, **C. Robin**, **A. Flores**, and **I. Dajani**, Experimental study of sbs suppression via white noise phase modulation. *In Fiber Lasers XI: Technology, Systems, and Applications*, volume 8961. International Society for Optics and Photonics, 2014.

7. **Boggio, J. C.**, **J. Marconi**, and **H. Fragnito** (2005). Experimental and numerical investigation of the sbs-threshold increase in an optical fiber by applying strain distributions. *Journal of Lightwave Technology*, **23**(11), 3808–3814.

8. **Bottrill, K.**, **R. Kakarla**, **F. Parmigiani**, **D. Venkitesh**, and **P. Petropoulos** (2015). Phase regeneration of qpsk signal in soa using single-stage, wavelength converting psa. *IEEE Photonics Technology Letters*, **28**(2), 205–208.

9. **Coles, J. B.**, **B.-P. Kuo**, **N. Alic**, **S. Moro**, **C.-S. Bres**, **J. C. Boggio**, **P. Andrekson**, **M. Karlsson**, and **S. Radic** (2010). Bandwidth-efficient phase modulation techniques for stimulated brillouin scattering suppression in fiber optic parametric amplifiers. *Optics Express*, **18**(17), 18138–18150.

10. **Connelly, M. J.**, *Semiconductor optical amplifiers*. Springer Science & Business Media, 2007.

11. **Cover, T. M.** and **J. A. Thomas**, *Elements of information theory*. John Wiley & Sons, 2012.

12. **Emmanuel, D.** and **M. Zervas** (1994). Erbium-doped fiber amplifiers: principles and applications.

13. **Engelbrecht, R.**, **M. Mueller**, and **B. Schmauss**, Sbs shaping and suppression by arbitrary strain distributions realized by a fiber coiling machine. *In 2009 IEEE/LEOS Winter Topicals Meeting Series*. IEEE, 2009.

14. **Grüner-Nielsen, L.**, **S. Dasgupta**, **M. D. Mermelstein**, **D. Jakobsen**, **S. Herstrøm**, **M. E. Pedersen**, **E. L. Lim**, **S.-u. Alam**, **F. Parmigiani**, **D. Richardson**, *et al.* (2010). A silica based highly nonlinear fibre with improved threshold for stimulated brillouin scattering. *paper Tu*, **4**, D3.

15. **Hansryd, J.**, **P. A. Andrekson**, **M. Westlund**, **J. Li**, and **P.-O. Hedekvist** (2002). Fiber-based optical parametric amplifiers and their applications. *IEEE Journal of Selected Topics in Quantum Electronics*, **8**(3), 506–520.

16. **Hansryd, J.**, **F. Dross**, **M. Westlund**, **P. Andrekson**, and **S. Knudsen** (2001). Increase of the sbs threshold in a short highly nonlinear fiber by applying a temperature distribution. *Journal of lightwave technology*, **19**(11), 1691.

17. **Hu, H.**, **R. Jopson**, **A. Gnauck**, **M. Dinu**, **S. Chandrasekhar**, **C. Xie**, and **S. Randel** (2015). Parametric amplification, wavelength conversion, and phase conjugation of a 2.048-tbit/s wdm pdm 16-qam signal. *Journal of Lightwave Technology*, **33**(7), 1286–1291.

18. **Hu, H.**, **E. Palushani**, **M. Galili**, **H. C. H. Mulvad**, **A. Clausen**, **L. K. Oxenløwe**, and **P. Jeppesen** (2010). 640 gbit/s and 1.28 tbit/s polarisation insensitive all optical wavelength conversion. *Optics express*, **18**(10), 9961–9966.

19. **Index, C. V. N.** (2017). Global mobile data traffic forecast update, 2016–2021 white paper. *Cisco: San Jose, CA, USA*.

20. **Jamshidifar, M.**, **A. Vedadi**, and **M. E. Marhic** (2009). Reduction of four-wave-mixing crosstalk in a short fiber-optical parametric amplifier. *IEEE Photonics Technology Letters*, **21**(17), 1244–1246.

21. **Jansen, S.**, **D. Van den Borne**, **B. Spinnler**, **S. Calabro**, **H. Suche**, **P. Krummrich**, **W. Sohler**, **G.-D. Khoe**, and **H. De Waardt** (2006). Optical phase conjugation for ultra long-haul phase-shift-keyed transmission. *Journal of Lightwave Technology*, **24**(1), 54.

22. **Jung, H.** (2011). Cisco visual networking index: global mobile data traffic forecast update 2010–2015. Technical report, Technical report, Cisco Systems Inc.

23. **Kalman, R. E.** (1960). A new approach to linear filtering and prediction problems. *Journal of basic Engineering*, **82**(1), 35–45.

24. **Karlsson, M.** (2016). Transmission systems with low noise phase-sensitive parametric amplifiers. *Journal of Lightwave Technology*, **34**(5), 1411–1423.

25. **Kurosu, T.**, **H. N. Tan**, **K. Solis-Trapala**, and **S. Namiki** (2015). Signal phase regeneration through multiple wave coherent addition enabled by hybrid optical phase squeezer. *Optics express*, **23**(21), 27920–27930.

26. **Labidi, T.**, **I. Fsaifes**, **W. Xie**, **D. Chatterjee**, **F. Goldfarb**, and **F. Bretenaker** (2018). Phase evolution of the direct detection noise figure of a nondegenerate fiber phase-sensitive amplifier. *Optics letters*, **43**(18), 4546–4549.

27. **Lali-Dastjerdi, Z.**, **M. Galili**, **H. C. H. Mulvad**, **H. Hu**, **L. K. Oxenløwe**, **K. Rottwitt**, and **C. Peucheret** (2013). Parametric amplification and phase preserving amplitude regeneration of a 640 gbit/s rz-dpsk signal. *Optics express*, **21**(22), 25944–25953.

28. **Leuthold, J.**, **C. Joyner**, **B. Mikkelsen**, **G. Raybon**, **J. Pleumeekers**, **B. Miller**, **K. Dreyer**, and **C. Burrus** (2000). 100 gbit/s all-optical wavelength conversion with integrated soa delayed-interference configuration. *Electronics Letters*, **36**(13), 1129–1130.

29. **Li, M.-J.**, **S. Li**, **D. A. Nolan**, **U. G. Achmetshin**, **M. M. Bubnov**, **A. N. Guryanov**, **E. M. Dianov**, **V. F. Khopin**, and **A. A. Sysoliatin**, New dispersion decreasing fiber with high sbs threshold for nonlinear signal processing. *In Optical Fiber Communication Conference*. Optical Society of America, 2005.

30. **Liu, X.**, **Y. Qiao**, and **Y. Ji** (2010). Reduction of the fiber nonlinearity impairment using optical phase conjugation in 40 gb/s co-ofdm systems. *Optics Communications*, **283**(13), 2749–2753.

31. **Madhow, U.**, *Fundamentals of digital communication*. Cambridge University Press, 2008.

32. **Mears, R. J.**, **L. Reekie**, **I. Jauncey**, and **D. N. Payne** (1987). Low-noise erbium-doped fibre amplifier operating at 1.54 μm. *Electronics Letters*, **23**(19), 1026–1028.

33. **Minzioni, P.**, **F. Alberti**, and **A. Schiffini** (2005). Techniques for nonlinearity cancellation into embedded links by optical phase conjugation. *Journal of lightwave technology*, **23**(8), 2364–2370.

34. **Minzioni, P.** and **A. Schiffini** (2005). Unifying theory of compensation techniques for intrachannel nonlinear effects. *Optics express*, **13**(21), 8460–8468.

35. **Moro, S.**, **A. Peric**, **N. Alic**, **B. Stossel**, and **S. Radic** (2010). Phase noise in fiber-optic parametric amplifiers and converters and its impact on sensing and communication systems. *Optics Express*, **18**(20), 21449–21460.

36. **Naimi, S. T.**, **S. P. Ó. Dúill**, and **L. P. Barry** (2014). Detailed investigation of the pump phase noise tolerance for wavelength conversion of 16-qam signals using fwm. *Journal of Optical Communications and Networking*, **6**(9), 793–800.

37. **Nesset, D.**, **T. Kelly**, and **D. Marcenac** (1998). All-optical wavelength conversion using soa nonlinearities. *IEEE Communications Magazine*, **36**(12), 56–61.

38. **Noe, R.** (2005). Pll-free synchronous qpsk polarization multiplex/diversity receiver concept with digital i&q baseband processing. *IEEE Photonics Technology Letters*, **17**(4), 887–889.

39. **Olsson, N. A.** (1989). Lightwave systems with optical amplifiers. *Journal of Lightwave Technology*, **7**(7), 1071–1082.

40. **Pedersen, B.**, **M. Dakss**, **B. Thompson**, **W. Miniscalco**, **T. Wei**, and **L. Andrews** (1991). Experimental and theoretical analysis of efficient erbium-doped fiber power amplifiers. *IEEE photonics technology letters*, **3**(12), 1085–1087.

41. **Premaratne, M.**, **D. Nešić**, and **G. P. Agrawal** (2008). Pulse amplification and gain recovery in semiconductor optical amplifiers: A systematic analytical approach. *Journal of Lightwave Technology*, **26**(12), 1653–1660.

42. **PriTel Inc** (2005). Optical fiber amplifiers FA-23. URL `https://www.pritel.com/low_power_fa.html`.

43. **Proakis, J.**, *Digital Communications*. McGraw-Hill series in electrical and computer engineering : communications and signal processing. McGraw-Hill, 2001. ISBN 9780071181839. URL https://books.google.co.in/books?id=aUp2QgAACAAJ.

44. **Puttnam, B. J.**, **D. Mazroa**, **S. Shinada**, and **N. Wada** (2011). Phase-squeezing properties of non-degenerate psas using ppln waveguides. *Optics express*, **19**(26), B131–B139.

45. **Savory, S. J.**, **G. Gavioli**, **R. I. Killey**, and **P. Bayvel** (2007). Electronic compensation of chromatic dispersion using a digital coherent receiver. *Optics express*, **15**(5), 2120–2126.

46. **Serena, P.**, **M. Salsi**, and **M. Bertolini** (2009). *Optilux Toolbox version 0.1 manual: the optical simulator toolbox*. URL http://optilux.sourceforge.net/Documentation/optilux_doc.pdf.

47. **Shao, J.** and **S. Kumar** (2012). Optical backpropagation for fiber-optic communications using optical phase conjugation at the receiver. *Optics letters*, **37**(15), 3012–3014.

48. **Shiraki, K.**, **M. Ohashi**, and **M. Tateda** (1996). Sbs threshold of a fiber with a brillouin frequency shift distribution. *Journal of Lightwave Technology*, **14**(1), 50–57. ISSN 0733-8724.

49. **Smith, R. G.** (1972). Optical power handling capacity of low loss optical fibers as determined by stimulated raman and brillouin scattering. *Appl. Opt.*, **11**(11), 2489–2494. URL http://ao.osa.org/abstract.cfm?URI=ao-11-11-2489.

50. **Sobhanan, A.**, **V. A. Karthik**, **L. V. Narayanan**, **R. D. Koilpillai**, and **D. Venkitesh**, Experimental analysis of noise transfer in optical phase conjugation process in nonlinear soa. *In Optical Fiber Communication Conference (OFC) 2019*. Optical Society of America, 2019. URL http://www.osapublishing.org/abstract.cfm?URI=OFC-2019-W2A.38.

51. **Sobhanan, A.** and **D. Venkitesh** (2018). Polarization-insensitive phase conjugation using single pump bragg-scattering four-wave mixing in semiconductor optical amplifiers. *Optics express*, **26**(18), 22761–22772.

52. **Solis-Trapala, K.**, **M. Pelusi**, **H. N. Tan**, **T. Inoue**, **S. Suda**, and **S. Namiki**, Doubled transmission reach for dp-64qam signal over field-deployed legacy fiber systems enabled by mssi. *In 2015 European Conference on Optical Communication (ECOC)*. IEEE, 2015.

53. **Steffensen, H.**, **J. R. Ott**, **K. Rottwitt**, and **C. McKinstrie** (2011). Full and semi-analytic analyses of two-pump parametric amplification with pump depletion. *Optics express*, **19**(7), 6648–6656.

54. **Tkach, R.**, **A. Chraplyvy**, and **R. Derosier** (1986). Spontaneous brillouin scattering for single-mode optical-fibre characterisation. *Electronics Letters*, **22**(19), 1011–1013.

55. **Wang, J.**, **A. Maitra**, **C. G. Poulton**, **W. Freude**, and **J. Leuthold** (2007). Temporal dynamics of the alpha factor in semiconductor optical amplifiers. *Journal of lightwave technology*, **25**(3), 891–900.

56. **Yaman, F.**, **Q. Lin**, **S. Radic**, and **G. P. Agrawal** (2005). Impact of pump-phase modulation on dual-pump fiber-optic parametric amplifiers and wavelength converters. *IEEE photonics technology letters*, **17**(10), 2053–2055.